Development 140, 3198-3209 (2013) doi:10.1242/dev.095448

Rho activation is apically restricted by Arhgap1 in neural crest cells and drives epithelial-to-mesenchymal transition

Matthew R. Clay and Mary C. Halloran*

SUMMARY

Epithelial-to-mesenchymal transitions (EMTs) are crucial for morphogenesis and carcinoma metastasis, yet mechanisms controlling the underlying cell behaviors are poorly understood. RhoGTPase signaling has been implicated in EMT; however, previous studies have yielded conflicting results regarding Rho function, and its role in EMT remains poorly understood. Elucidation of precise Rho functions has been challenging because Rho signaling is highly context dependent and its activity is tightly regulated spatiotemporally within the cell. To date, few studies have examined how Rho affects cell motility in intact organisms, and the pattern of Rho activity during motile cell behaviors of EMT has not been determined in any system. Here, we image endogenous active Rho during EMT *in vivo*, and analyze effects of Rho and Rho-kinase (ROCK) manipulation on cell motility *in vivo*. We show that Rho is activated in a discrete apical region of premigratory neural crest cells during EMT, and Rho-ROCK signaling is essential for apical detachment and generation of motility within the neuroepithelium, a process that has been poorly understood. Furthermore, we find that Arhgap1 restricts Rho activation to apical areas, and this restriction is necessary for detachment. Our results provide new insight into mechanisms controlling local Rho activation and how it affects dynamic cell behaviors and actomyosin contraction during key steps of EMT in an intact living organism.

KEY WORDS: EMT, RhoGTPase, Neural crest, GAP, Zebrafish

INTRODUCTION

Epithelial-to-mesenchymal transitions (EMTs) are extremely important for tissue remodeling during embryonic development, and are central events in several pathologies, including cancer in humans (Hay, 1995; López-Novoa and Nieto, 2009; Shook and Keller, 2003; Thiery et al., 2009). EMT is a distinctive cell motility process in which an epithelial cell converts to a migratory cell, and which involves complex changes in cell morphology, cytoskeletal dynamics and cadherin-based cell adhesions (Duband et al., 1995; Hay, 1995; Shook and Keller, 2003). However, the mechanisms regulating these changes within epithelial tissues, especially *in vivo*, remain poorly understood, in part because few studies have examined the effects of molecular manipulation on the motile cell behaviors underlying EMT in intact systems.

Small GTPases of the Rho family play important roles in regulating cytoskeletal dynamics, cell adhesions and motility during many cellular processes (Jaffe and Hall, 2005). The GTPase Rho has known functions in cell migration, but its role in the unique process of EMT and the initiation of motility within an epithelium remains unclear (Clay and Halloran, 2011; Nieto, 2002; Thiery et al., 2009). Conflicting results of Rho function have come from previous studies, with some concluding that Rho stimulates EMT (Bakin et al., 2000; Berndt et al., 2008; Bhowmick et al., 2001; Cho and Yoo, 2007; Liu and Jessell, 1998; Masszi et al., 2003) while others conclude that it inhibits EMT (Groysman et al., 2008; Nakaya et al., 2008; Ozdamar et al., 2005; Shoval and Kalcheim, 2012). These conflicting results likely reflect the fact that Rho signaling is highly context dependent. Indeed, in several cases tumor cell invasion, an outcome of EMT, can be stimulated by Rho or its effector Rho Kinase (ROCK) (Croft et al., 2004; Peng et al., 2012; Wilkinson et al., 2005), but cells can switch between ROCK-dependent and -independent invasion depending on context (Sahai and Marshall, 2003). Furthermore, Rho can regulate different processes in distinct subcellular locations (Guilluy et al., 2011; Jaffe and Hall, 2005; Samarin and Nusrat, 2009), and is strongly influenced by extracellular cues (Lessey et al., 2012; Provenzano and Keely, 2011), which can be disrupted in *in vitro* EMT models. To define precise functions of Rho in a complex process such as EMT, it is crucial to determine where and when Rho is activated within the cell, how these patterns are established and how Rho mediates specific behaviors in intact systems.

The specific subcellular localization and level of Rho activity are dictated by numerous regulators. RhoGTPases can be activated by guanine nucleotide exchange factors (GEFs) and inactivated by GTPase-activating proteins (GAPs). Interestingly, the GEFs and GAPs greatly outnumber the Rho proteins. For example, more than 70 RhoGAPs have been identified in various species (Tcherkezian and Lamarche-Vane, 2007). The existence of so many GAPs is itself evidence that RhoGTPase activity and spatiotemporal distribution are tightly regulated and crucial to function. However, very little is known about which GAP family members regulate particular cellular processes and how they sculpt localized GTPase activity during cell motility. The founding member of the RhoGAP family, Arhgap1 (aka RhoGAP, p50RhoGAP, Cdc42GAP), has biochemical GAP activity towards Cdc42 and Rho (Barfod et al., 1993; Ridley et al., 1993; Zhang and Zheng, 1998), and loss-of-function studies suggest diverse functions. Arhgap1 knockout mice have increased apoptosis (Wang et al., 2005), decreased wound healing and decreased migration of fibroblasts and hematopoietic cells (Wang et al., 2006; Yang et al., 2006). In cancer cells, Arhgap1 is a potential target of both oncogenic and tumor suppressive microRNAs (Ahn et al., 2012; Ouchida et al., 2012) and is necessary for TGF-β-

Cell and Molecular Biology Program, University of Wisconsin, Madison, WI 53706, USA. Department of Zoology, University of Wisconsin, Madison, WI 53706, USA. Department of Neuroscience, University of Wisconsin, Madison, WI 53706, USA.

*Author for correspondence (mchalloran@wisc.edu)

Accepted 23 May 2013

induced invasion (Ahn et al., 2012). Similar to the RhoGTPases themselves, their GAP modulators may regulate multiple processes and are likely influenced by cellular context. To date, specific functions for Arhgap1 in cell motility are poorly understood, and roles in EMT have not been described. Moreover, how Arhgap1 patterns localized Rho activity during motility processes is unknown.

Zebrafish neural crest cells (NCCs) are an excellent model with which to study EMT *in vivo*. EMT is a crucial step in NCC development and is required for migration (Le Douarin and Kalcheim, 1999). Here, we image the subcellular localization of endogenous active Rho and F-actin as NCCs undergo EMT in intact embryos. We show that Rho is activated and F-actin is enriched apically in premigratory NCCs during apical detachment, an initial step required for EMT. We find that Rho, ROCK and myosin II are required for detachment and EMT. Furthermore, we show that Arhgap1 restricts Rho activation during apical detachment. Arhgap1 knockdown results in broader Rho activation and prevents apical detachment and EMT. Together, these data reveal a previously unknown mechanism in which Arhgap1 focuses Rho activation to a specific subcellular area, which in turn promotes localized ROCK-driven actomyosin contraction that triggers specific cell motility behaviors essential for EMT.

MATERIALS AND METHODS

Animals

Zebrafish (*Danio rerio*) embryos were obtained from wild-type (AB) matings. Embryos were raised in E3 embryo medium at 23-28.5°C and staged as described (Kimmel et al., 1995). Animal work was carried out in compliance with United States Department of Health and Human Services guidelines, and the animal use protocol was approved by the University of Wisconsin Institutional Animal Care and Use Committee.

DNA constructs, mRNA synthesis, morpholinos and embryo microinjection

DNA plasmids were generated using Gateway (Invitrogen) or In-Fusion (Clontech) cloning into tol2 (Kwan et al., 2007) or pCS2 vectors, respectively. The Rho biosensor (GFPrGBD) (Benink and Bement, 2005), utrophin F-actin biosensor (mCherry-UtrCH) (Burkel et al., 2007), mCherry, prenylated GFP (GFP-CAAX) or prenylated mCherry (mCherry-CAAX) were Gateway cloned behind a 4.9 kb fragment from the regulatory element of the NCC specific gene *sox10* (*-4.9sox10*) (Wada et al., 2005). Arhgap1 was cloned behind GFP into pCS2. To mosaically label NCCs, 12.5-25 pg DNA was injected at the one-cell stage as described previously (Andersen et al., 2010) with 25 pg *tol2* mRNA in a volume of 1 nl. mRNA encoding Pard3-GFP or GFP-Arhgap1 was synthesized with mMessage (Life Technologies) and 70-150 pg was injected at the one- to two-cell stage. Morpholinos were synthesized by Gene Tools (Corvalis, OR) and injected at the one-cell stage. Arhgap1MO1 (5′-AGCAAGAGTTAT-GGTGCCTACATGA-3′) or Arhgap1MO2 (5′-GTCACCTGTAA-AGGAGACAGATTAA-3′) were injected at 500-750 μM in a 1 nl volume. For live imaging, a p53 morpholino (5′-GCGCCATTGC-TTTGCAAGAATTG-3′) was co-injected at 250 μM. A standard scrambled morpholino was used as a control: 5′-CCTCTTACCTCAG-TTACAATTTATA-3′.

Time lapse confocal imaging

Embryos showing intermediate levels of probes or markers were selected for imaging and mounted in 1% low-melting point agarose in E3 with 10 mM HEPES in imaging chambers as described previously (Andersen et al., 2010). Imaging was carried out on an Olympus FV1000 laser-scanning confocal microscope using a 60× oil immersion objective (NA 1.35), and began at 14 hpf when hindbrain NCCs are at varying stages of EMT. Cells were selected from rhombomeres 1-4 based on the following criteria: for apical detachment, we chose NCCs in contact with both the apical midline and the basal edge of the neuroepithelium, and acquired images every 30 seconds; for blebbing, we chose NCCs that had lost their apical attachments and begun rounding, and acquired images every 10 seconds. For ratiometric imaging, acquisition parameters were optimized to ensure GFP and mCherry were below saturation. To label apical regions, we injected *pard3-GFP* mRNA into one- to two-cell embryos.

Imaging analysis and statistics

Volocity software (Perkin Elmer) was used for ratiometric analysis of the Rho biosensor. Z-stacks were merged using a brightest point accumulation and noise was removed from both channels using a fine filter. Background was subtracted and the software calculated each channel threshold. GFP/mCherry intensity was created as a new channel based on a rainbow look-up table.

In blebs, we measured active Rho in a region of interest (ROI) drawn around the membrane of a retracting bleb, and an ROI-containing adjacent, non-blebbing membrane. The GFP/mCherry intensity in the ROIs was averaged over time during bleb retraction. For individual blebs, average GFP/mCherry intensity was compared between the two ROIs using paired, one-tailed *t*-tests. Owing to subtle differences in expression levels and acquisition parameters between embryos, we did not use GFP/mCherry for comparisons between embryos. Instead, we created a normalized measure of active Rho we termed R-value by dividing GFP/mCherry intensity in the bleb ROI by that in the non-blebbing membrane ROI. Values above one indicate higher active Rho in the bleb. For each bleb we averaged R-values over time, made pairwise comparisons between blebs using Tukey's pairwise multiple comparisons test, and calculated an average R-value for the population of NCCs.

During apical detachment, R-values were calculated by dividing the GFP/mCherry intensity of a five-pixel diameter ROI in the NCC tail by that in an ROI at the NCC leading edge. In individual NCCs, we calculated R-values for each time point and defined three periods for analysis. 'Before EMT' included time points from 60 minutes to 40 minutes before apical detachment. 'During EMT' included 10 minutes before apical detachment until the NCC completely segregated from the neuroepithelium. 'After EMT' included all times after the NCC delaminated and began to migrate away from the neuroepithelium. We calculated the population average R-value during these periods and compared 'during' versus 'after' EMT using a paired, two-tailed *t*-test and compared 'before', 'during' and 'after' EMT using Tukey's multiple comparisons test. Comparisons between R-values from NCCs in wild-type and Arhgap1 morpholino-injected embryos were made using an unpaired, two-tailed *t*-test.

To determine the proportion of cell area in which Rho was activated, we calculated the average maximum GFP/mCherry intensity in the cell over the time. For wild-type NCCs this was 20 minutes, beginning 10 minutes before detachment. For NCCs in Arhgap1 knockdown embryos, this was 20 minutes beginning when Rho activation was first observed. We set a threshold at one-third the average maximum, determined the proportion of the cell area with GFP/mCherry above this threshold, and averaged this value over the 20 minutes. Comparison of active Rho area between wild-type and Arhgap1 knockdown was carried out using an unpaired, two-tailed, *t*-test.

All kymographs were generated in Volocity by drawing a line spanning the area of interest in confocal *z*-projections. To quantify active Rho during apical detachment, a line was drawn on the kymograph at the cell border for the NCC tail and leading edge. GFP/mCherry along this line was normalized to the highest observed value, and averaged. In individual NCCs, these values were compared using paired, two-tailed *t*-tests.

In NCCs labeled with GFP-CAAX, we calculated the proportion of NCCs undergoing EMT. Only cells in the neuroepithelium at the onset of imaging were counted, and cells were considered to complete EMT after the entire cell had delaminated from the neuroepithelium. Comparisons between groups were made with Fisher's exact tests.

Inhibitor treatments

Embryos were dechorionated and incubated in pharmacological inhibitors diluted in E3 buffered with 10 mM HEPES at the following concentrations: 2 μg/ml C3 (Cytoskeleton), 50 μM ROCKout (EMD Millipore) with 4% DMSO and 50 μM (–)-blebbistatin (Sigma) with 4% DMSO. For live

imaging, embryos were pre-treated for 2 hours (C3) or 30 minutes (ROCKout) prior to mounting, and treated throughout imaging.

Scoring of cell morphology

For cell morphology analysis, embryos were injected with *-4.9sox10:GFP-CAAX* DNA at the one-cell stage. Embryos were treated with ROCKout or blebbistatin from 14-16 hpf or C3 from 12-16 hpf, and fixed with 4% paraformaldehyde at 16 hpf. For Arhgap1 knockdown, embryos were injected with *-4.9sox10:GFP-CAAX* DNA and control or Arhgap1 morpholino and fixed at 16 hpf. Embryos were incubated with rabbit anti-GFP primary antibody (1:1000, Life Technologies) followed by Alexa-488 goat anti-rabbit IgG (1:1000, Life Technologies) secondary. Embryos were mounted in 70% glycerol. Images of the hindbrain were acquired on a Nikon TE3000 microscope with a 40× objective using MetaMorph software (Molecular Devices). Cell morphology in rhombomeres 1-4 was scored by experimenters blinded to treatments. Labeled cells were counted as elongated if they contacted both the apical midline and the basal surface, determined from overlays of fluorescent and DIC images. After scoring, cells from like treatments were pooled and the proportion of NCCs with an elongated morphology was determined. Comparisons between treatments were made using Fisher's exact tests.

Statistical analysis

All statistics were calculated with Prism 5.0 (GraphPad Software). For box plots: line is median, + is mean, box covers upper and lower quartiles, and bars encompass minimum and maximum.

RESULTS

Premigratory NCCs span the neuroepithelium from apical to basal surfaces before undergoing a series of stereotyped EMT behaviors and then beginning directed migration away from the neuroepithelium (Fig. 1A). One of the first discernible behaviors of NCC EMT is the detachment of the cell 'tail' from the apical midline, which is preceded by or coincides with loss of apical cell junction components (Ahlstrom and Erickson, 2009). After detachment the trailing tail continues to retract as the cell rounds at the basal side of the neuroepithelium where it begins membrane blebbing and subsequently delaminates (Berndt et al., 2008). We previously showed that blebbing and exit from the neuroepithelium depend on ROCK and myosin II (Berndt et al., 2008). However the molecular mechanisms that control apical detachment and initiate EMT have been poorly understood.

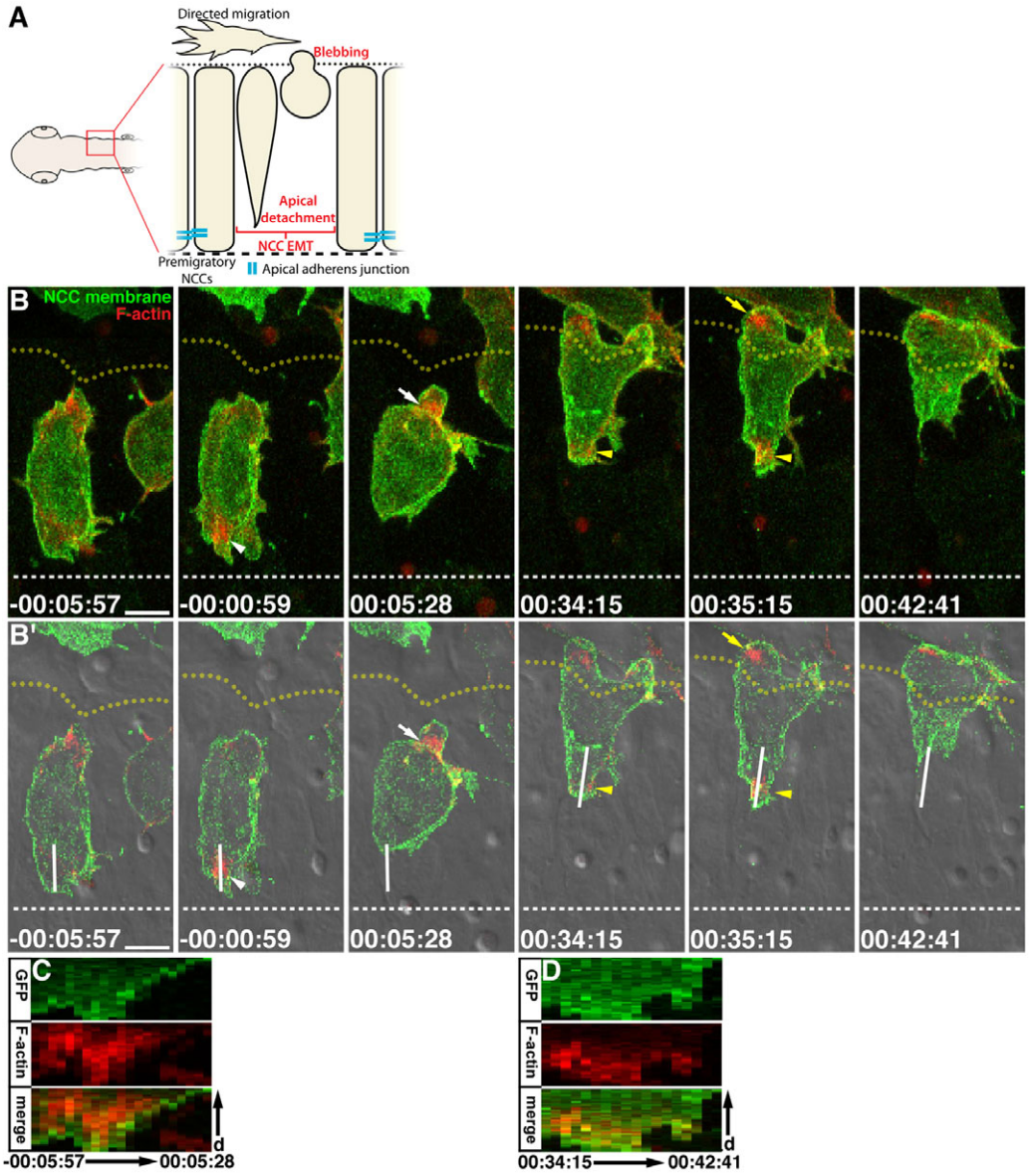

Fig. 1. F-Actin transiently accumulates in NCC tails prior to detachment and retraction. (**A**) Imaging region and steps of EMT. (**B**,**B′**) Time lapse images (dorsal views, anterior left) of an NCC labeled with GFP-CAAX and mCherry-UtrCH. Yellow dotted lines mark basal neuroepithelial surface. White dashed lines mark apical midline. Apical detachment is 0 minutes. (B) Confocal *z*-projection. (B′) *Z*-projection of fluorescence over a single DIC plane, showing lines for kymographs. F-actin increases in apical tail prior to detachment (white arrowhead) and during later tail retraction (yellow arrowheads). Blebs protrude away from underlying F-actin (white arrows), which fills blebs as they retract (yellow arrow). (**C**,**D**) Kymographs showing GFP-CAAX and mCherry-UtrCH. Scale bars: 10 μm. Time is given as hours:minutes:seconds.

F-actin accumulates in apical NCC tails during EMT

F-actin and myosin II (actomyosin) contractile forces are important for many cell motility processes (Martin, 2010). To determine whether actomyosin is involved in apical detachment, we imaged F-actin during early stages of EMT. We mosaically labeled NCCs with membrane-targeted GFP (GFP-CAAX*)* and an F-actin biosensor (mCherry-UtrCH) (Berndt et al., 2008; Burkel et al., 2007) that allows visualization of individual cells. We began imaging before apical detachment, when NCCs spanned the apical-basal extent of the neuroepithelium. We used the embryonic midline, visible with DIC optics, to identify the apical surface. In all NCCs analyzed (*n*=7), we found transient accumulations of F-actin beneath the membrane prior to apical detachment that move forward as the tail translocates and dissipate near the end of retraction (Fig. 1B,B′, white arrowheads; Fig. 1C; supplementary material Movie 1). Following apical detachment, before the next tail retraction within the neuroepithelium, F-actin again accumulates in the tail and cycles similarly to initial detachment (Fig. 1B,B′, yellow arrowheads; Fig. 1D; supplementary material Movie 1). Because we see F-actin in tails not only during initial detachment, but also during later retractions, we are likely visualizing F-actin specifically associated with tail detachment and retraction, rather than with adherens junctions prior to initial detachment.

To test our method to identify the apical surface and thus corroborate that we are imaging apical detachment, we labeled embryos with the apical marker Pard3-GFP. We also mosaically labeled NCCs and asked whether NCC tails with midline contact, based on DIC, were indeed apical (supplementary material Fig. S1). Most NCCs classified as having midline contact showed Pard3-GFP near the midline (Table 1). Importantly, in all cases where premigratory NCCs lacked Pard3-GFP, a neighboring cell had Pard3-GFP in the same region as the NCC tail, indicating it was indeed in the apical neuroepithelium. Overall, these results show that we can image the early steps of EMT *in vivo* and that F-actin distribution is tightly regulated at the apical side of NCCs during detachment in a manner consistent with actomyosin contraction promoting this process.

Rho biosensor imaging reveals specific subcellular activation during NCC EMT

Rho activation is often upstream of actomyosin contraction (Jaffe and Hall, 2005). To better define Rho functions in EMT, we asked where Rho is activated during EMT behaviors. We imaged active Rho with a biosensor consisting of the Rho-binding domain of Rhotekin (rGBD), fused to GFP (Benink and Bement, 2005) (GFP-rGBD), which has the advantage of labeling endogenous Rho and accurately reports active Rho localization in multiple systems (Bement et al., 2005; Benink and Bement, 2005; Godsel et al., 2010; Miller and Bement, 2009; Nakaya et al., 2008; Rohani et al., 2011; Vaughan et al., 2011; von Dassow et al., 2009; and see below). We labeled NCCs with GFP-rGBD and cytosolic mCherry as a volume marker, and performed ratiometric imaging. NCCs expressing the biosensor exhibited characteristic behaviors of EMT, exited the neuroepithelium and initiated migration; thus, the biosensor did not appear to affect normal NCC behaviors. We first tested the Rho biosensor during NCC blebbing, a behavior known to require ROCK (Berndt et al., 2008). Indeed, we found that Rho is activated as blebs approach maximal extension and remains elevated as they retract (Fig. 2B-D; supplementary material Movie 2). In most cases, the ratio of GFP-rGBD to mCherry (GFP/mCherry) in retracting bleb membrane was significantly higher than adjacent non-blebbing membrane. (supplementary material Fig. S2; Table S1). Across the NCC population, the average GFP/mCherry intensity in retracting blebs normalized to non-blebbing membrane (referred to as R-value, see Materials and methods; supplementary material Fig. S2) showed active Rho was 52% higher in blebs during retraction (Fig. 2E). Comparisons between blebs showed no differences, suggesting Rho activation in blebs is tightly controlled. This pattern of active Rho is similar to the dynamic pattern of F-actin we previously reported in blebs (Berndt et al., 2008), suggesting the result of Rho activation in NCC blebs is to promote actomyosin and bleb retraction.

To test whether Rho is activated during initial apical detachment, a behavior where F-actin is also concentrated (see Fig. 1), we imaged active Rho during early EMT. We found that Rho is activated in NCC apical tails prior to detachment, and remains activated as EMT proceeds (Fig. 3B; supplementary material Movie 3). Comparisons of GFP/mCherry intensity from kymographs during retraction (Fig. 3C,C′,D,D″; supplementary material Fig. S3) showed that in all cases active Rho was higher in the tail relative to the leading edge (supplementary material Table S2). Analysis of active Rho level in the tail normalized to the leading edge (R-value, see Materials and methods; supplementary material Fig. S3) showed that in individual NCCs, Rho activation was highest just prior to and during apical detachment, and lowest after NCCs had delaminated from the neuroepithelium (Fig. 3E,G; supplementary material Fig. S3). We analyzed active Rho levels across the NCC population during two time periods: ‘during EMT’ and ‘after EMT’ (see Materials and methods). During EMT, active Rho was 62% higher in tails relative to the leading edge (Fig. 3F). After EMT, the average active Rho signal was reduced, yet still 35% higher in the tail relative to the leading edge.

To determine whether Rho is activated specifically during EMT, we measured active Rho in premigratory NCCs at an earlier stage, from 60 to 40 minutes before apical detachment (Fig. 3G). The average active Rho level in apical tails during this period was significantly lower than during EMT, and was similar to levels after EMT (Fig. 3H). These data show the higher level of active Rho in apical tails is specific to detachment and EMT, and support the idea that Rho promotes these processes.

Rho inhibition eliminates Rho biosensor localization and disrupts NCC EMT *in vivo*

To confirm the specificity of the Rho biosensor and test the function of Rho in NCC apical detachment, we treated embryos with C3 exotransferase to inhibit Rho activation. C3 treatment eliminated all specific subcellular localization of biosensor signal (Fig. 4B,C). The population average of active Rho level was significantly lower than in untreated embryos (Fig. 4D). These data indicate that the biosensor provides a specific readout of active Rho in NCCs. To test whether Rho activation is required

Table 1. Number of premigratory NCCs expressing apical Pard3-GFP near the midline

Number of premigratory NCCs (number of embryos)	Pard3-GFP-positive NCCs	Pard3-GFP observed within 5 μm of midline	Pard3-GFP observed beyond 5 μm of midline (average distance)
39 (6)	32/39 (82.1%)*	30/32 (93.8%)	2/32 (6.95 μm)

*In each case where NCCs lacked Pard3-GFP, an adjacent cell expressed Pard3-GFP near the midline.

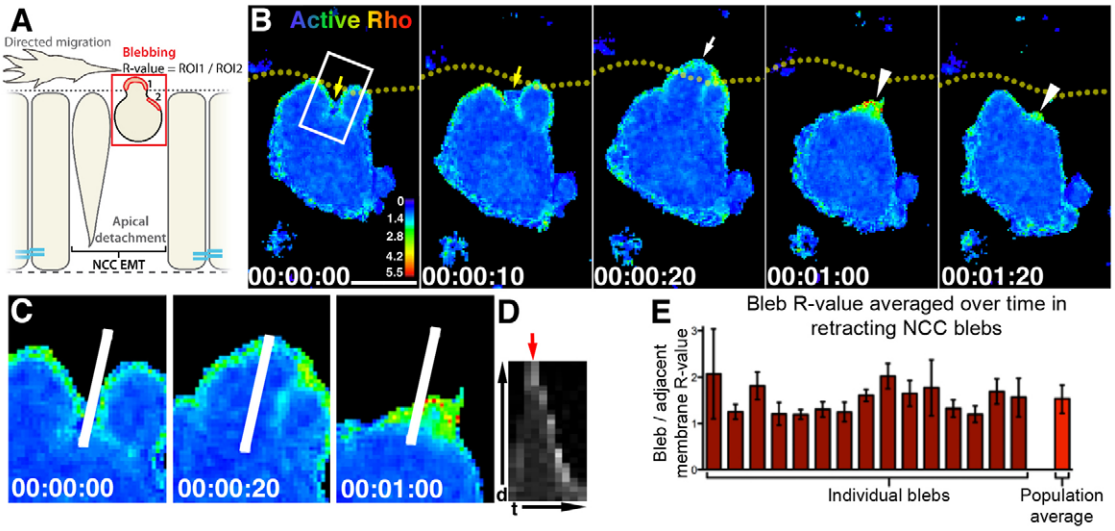

Fig. 2. Active Rho is elevated in retracting NCC blebs. (**A**) Schematic showing imaging region. (**B**) Time-lapse images (dorsal views, anterior left, confocal *z*-projections) of an NCC expressing GFPrGBD and mCherry. Yellow arrow indicates forming bleb. Rho is activated at maximal bleb extension (white arrow) and in retracting blebs (arrowheads). Box outlines area shown in C. Look-up table shows GFP/mCherry intensity. Yellow dotted lines mark basal neuroepithelial surface. (**C**) Higher magnification of bleb showing line for kymograph. (**D**) Kymograph of GFP/mCherry. Red arrow indicates maximal bleb extension. (**E**) Active Rho R-values in retracting blebs (ROI in bleb/ROI in non-bleb membrane, see supplementary material Fig. S1). R-values above 1.0 indicate Rho activation. Pairwise comparisons (Tukey's multiple comparisons test) showed no differences between blebs. Scale bar: 10 μm. Time is given as hours:minutes:seconds.

for apical detachment and EMT, we mosaically labeled NCCs with GFP-CAAX and imaged during C3 treatment. NCCs maintained an elongated morphology similar to premigratory NCCs, and most did not undergo detachment during C3 treatment (Fig. 5B; supplementary material Movie 4). Only 25.6% of labeled NCCs completed EMT (average imaging time 140.2 minutes), compared with 77.2% in untreated embryos (average imaging time 112.5 minutes) (Fig. 5D). Only NCCs that began in the neuroepithelium were scored and EMT was considered complete when the entire cell was outside of the neuroepithelium. To assess detachment, we scored cell morphology in embryos treated with C3 and fixed at 16 hpf. Rho inhibition caused a substantial increase in the proportion of NCCs that spanned the entire apicobasal width of the neuroepithelium, i.e. cells maintaining a premigratory morphology (Table 2). Together, these data show that Rho activity is necessary for apical tail detachment.

ROCK or myosin II inhibition disrupts NCC EMT

To identify molecules downstream of Rho that promote detachment and EMT, we tested the roles of ROCK and myosin II. We mosaically labeled NCCs with GFP-CAAX and treated embryos with a ROCK inhibitor (ROCKout). Most of the labeled NCCs located in the neuroepithelium at imaging onset maintained apical contact (Fig. 5C; supplementary material Movie 5) and did not undergo EMT (86.2% failed to complete EMT; Fig. 5D). During ROCKout treatment, NCCs exhibited some protrusive behavior near the midline (Fig. 5C′; supplementary material Movie 5), which resembled behaviors reported in other neuroepithelial cells (Hong and Brewster, 2006), but did not display EMT-associated blebbing at the basal surface. We further quantified the effects of ROCK or myosin II inhibition on apical detachment by scoring cell morphology in embryos fixed at 16 hpf. Inhibition of ROCK or myosin II significantly increased the proportion of NCCs spanning the neuroepithelium (Table 2), indicative of failure to initiate apical detachment. Importantly, NCCs that were outside the neuroepithelium at imaging onset during ROCKout treatment were capable of directed migration (Fig. 5C, arrowheads; supplementary material Movie 5), a behavior associated with lower active Rho levels (Fig. 3F,H). In addition, premigratory NCCs could undergo cell divisions during ROCKout treatment, although both cells remained near the apical midline throughout cytokinesis and did not detach following division (supplementary material Movie 5). Thus, this degree of ROCK inhibition disrupts only a subset of NCC behaviors, detachment and blebbing (Berndt et al., 2008), associated with the highest relative levels of active Rho, suggesting EMT is dependent on higher levels of Rho-ROCK signals than cell division or directed NCC migration. Together, these data show that ROCK and myosin II are required for apical detachment and EMT, and suggest Rho-ROCK-mediated actomyosin contraction drives these behaviors.

To determine whether Rho-ROCK signaling is required for apical F-actin accumulation, we imaged with the F-actin biosensor during C3 or ROCKout treatment. We found that F-actin still accumulated in the apical tail of NCCs after inhibition of Rho (9/10 NCCs in three embryos) or ROCK (8/8 NCCs in four embryos) (Fig. 5E,F). These results suggest that Rho signaling is not necessary for initial F-actin polymerization, but only for the ROCK-mediated actomyosin contractile forces that act on F-actin to drive detachment.

Arhgap1 restricts Rho activity and is required for apical detachment

We next sought to determine what mechanisms control active Rho localization during EMT. Arhgap1 was selected as a candidate because it is expressed in the central nervous system at NCC EMT stages (Thisse and Thisse, 2004). We tested two splice-blocking morpholinos designed to knock down Arhgap1. Both morpholinos caused deletion of all or part of exon 4, which led to a reading frame shift and premature stop (supplementary material Fig. S4), and both showed similar effects on NCCs (see below). We selected the

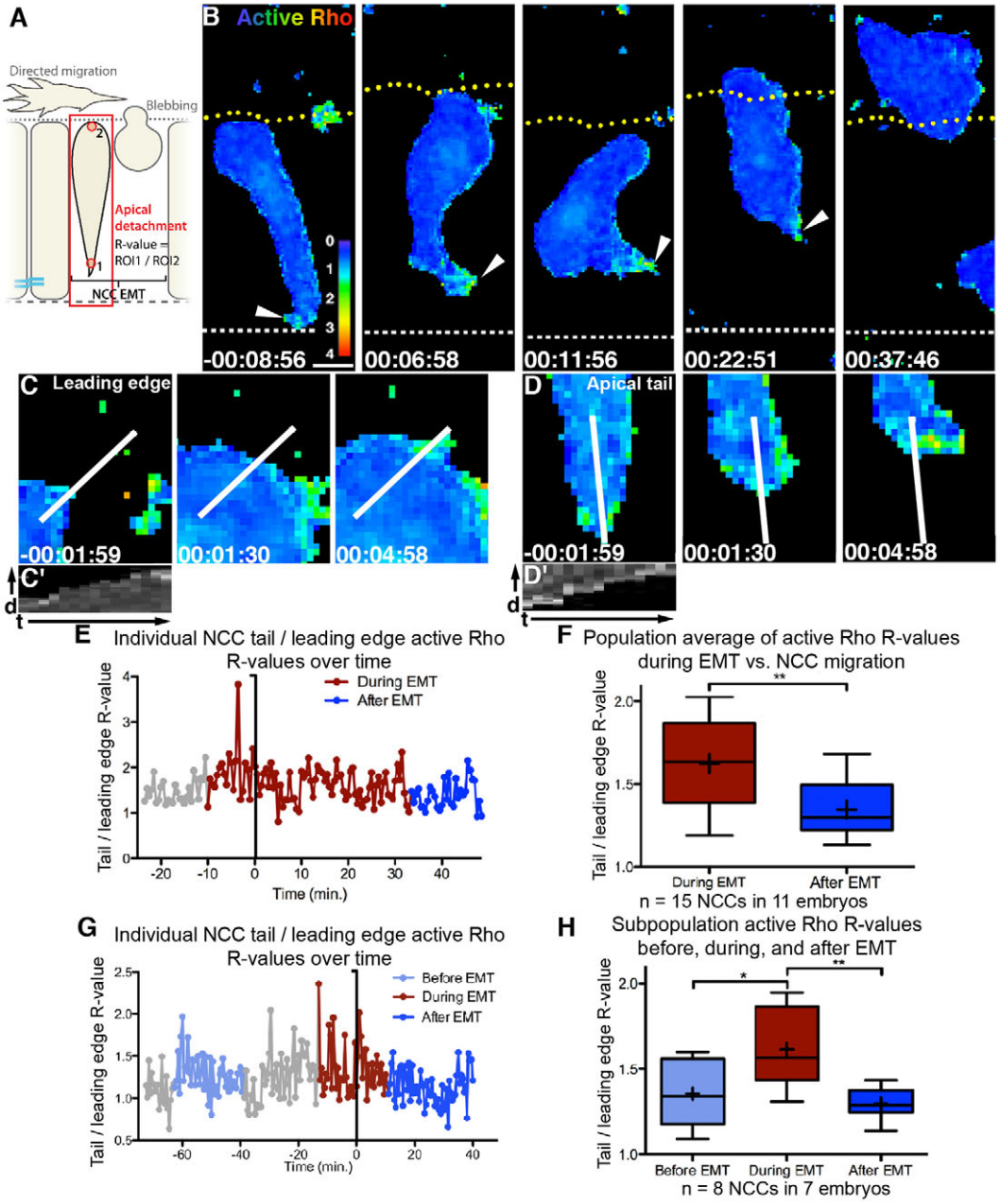

Fig. 3. Active Rho is elevated in retracting NCC tails. (**A**) Imaging region. (**B**) Time-lapse images (dorsal views, anterior left, confocal z-projections) of an NCC expressing GFPrGBD and mCherry. Rho is activated during tail detachment and retraction (arrowheads). Look-up table shows GFP/mCherry intensity. Yellow dotted lines mark basal neuroepithelial surface. White dashed lines mark apical midline. In B-D,E,G), detachment is 0 minutes. (**C**,**D**) Zoom views of leading edge (C) and apical tail (D) showing lines for kymographs. (C′,D′) Kymographs of GFP/mCherry. (**E**) Tail/leading edge active Rho R-value over time for NCC in B. Gray plots before EMT are not included in F. (**F**) Population average of active Rho R-values (***P*<0.01, paired two-tailed, *t*-test). (**G**) Plot of individual NCC R-Value starting 70 minutes before detachment. Gray plots not included in H. (**H**) Subpopulation average of active Rho R-values (**P*<0.05,***P*<0.01, Tukey's multiple comparisons test). Scale bar: 10 µm. Time is given as hours:minutes:seconds.

morpholino with more efficient exon exclusion (MO1, supplementary material Fig. S4) for live imaging experiments.

To test whether Arhgap1 affects the level, timing or pattern of Rho activation in NCCs, we imaged the Rho biosensor in Arhgap1 morpholino-injected embryos. We found that Rho was activated to similar levels as in wild-type embryos (R-value=1.50 in Arhgap1 knockdown versus R-value=1.62 in wild type); however, the area of Rho activation appeared broader in Arhgap1 knockdown NCCs (Fig. 6B; supplementary material Movie 6). We calculated the proportion of the total NCC area occupied by the highest active Rho signal (see Materials and methods) and found that Arhgap1 knockdown caused expansion in the area of Rho activation (Fig. 6C). To examine the effects of Arhgap1 knockdown and expanded Rho activation on apical detachment and EMT, we labeled NCCs with GFP-CAAX and performed live imaging after Arhgap1 knockdown. Most NCCs remained elongated, did not detach, and failed to undergo EMT in Arhgap1 knockdown embryos (Fig. 6D), with only 38.9% of NCCs completing EMT compared

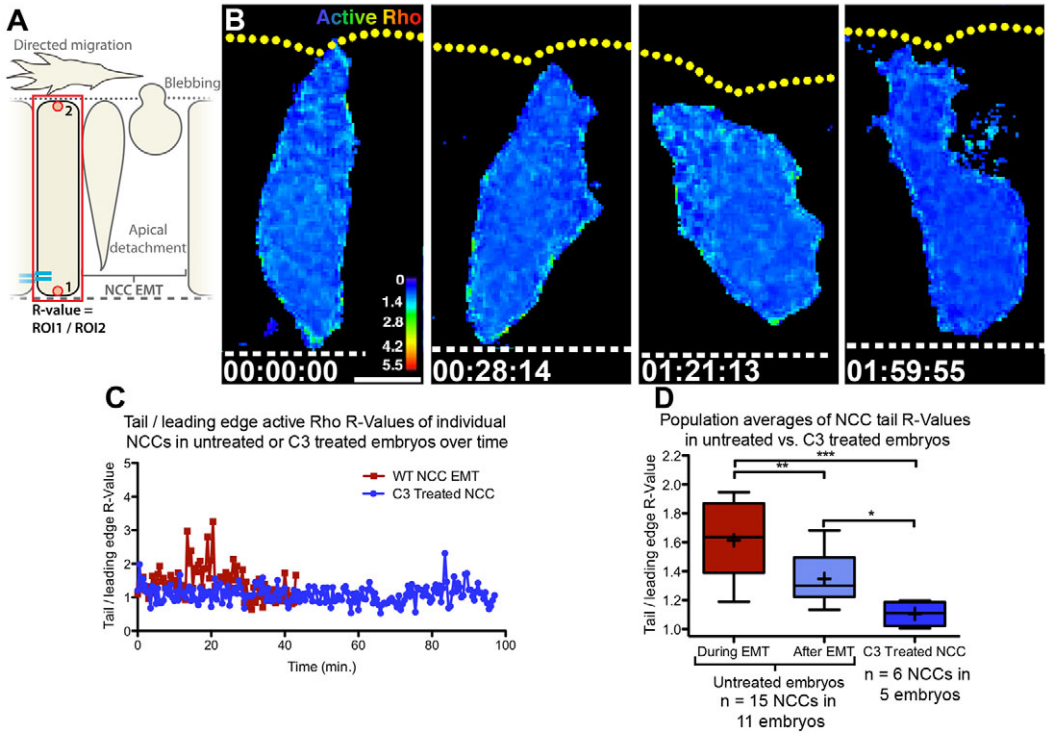

Fig. 4. C3 treatment eliminates active Rho localization. (**A**) Imaging region. (**B**) Time-lapse images (dorsal views, anterior left, confocal *z*-projections) of an NCC labeled with GFPrGBD and mCherry and treated with C3. The cell shows no distinct active Rho localization and fails to undergo EMT over 3 hours. Look-up table shows GFP/mCherry intensity. Yellow dotted lines mark basal neuroepithelial surface. White dashed lines mark apical midline. (**C**) Active Rho NCC tail R-values for individual NCC in C3-treated embryo over time (blue). NCCs from untreated embryos shown for reference (red). (**D**) Population average of active Rho R-values (***P<0.001, **P<0.01, *P<0.05, Tukey's multiple comparisons test). Scale bar: 10 μm. Time is given as hours:minutes:seconds.

with 71.2% in control morpholino injected embryos (Fig. 6E). We scored the proportion of NCCs spanning the neuroepithelium in embryos fixed at 16 hpf, and found a significant increase in NCCs with premigratory morphology after Arhgap1 knockdown (Table 2). We observed this phenotype with two separate morpholinos (Table 2), suggesting the phenotype was not due to non-specific effects.

Interestingly, we found that the timing of Rho activation was similar between Arhgap1 knockdown and wild-type embryos. Arhgap1 knockdown NCCs showed an early phase of lower active Rho followed by higher Rho activation. On average, the increase occurred 53.1 minutes into imaging, similar to when Rho activity increased during EMT in wild-type NCCs (average 41.8 minutes into imaging). Together, these data indicate that Arhgap1 does not affect the timing of Rho activation, but is instead required to inhibit Rho activity in basolateral cell areas and thus focus Rho activity to the most apical cell region. Our finding that Rho inhibition and Arhgap1 knockdown cause similar phenotypes also suggests that the proper distribution of Rho signal is crucial, and that focusing Rho activation is necessary for apical detachment and NCC EMT.

To assess the spatial distribution of Arhgap1 protein, we expressed a GFP-Arhgap1 fusion protein in all cells. Hindbrain neuroepithelial cells showed GFP-Arhgap1 throughout the cytoplasm and in puncta resembling vesicles (Fig. 6F), consistent with a report of Arhgap1 in endosomes (Sirokmány et al., 2006). In a minority of premigratory NCCs (21.7%), GFP-Arhgap showed lower levels in the apical region (Fig. 6G), whereas most premigratory NCCs showed a more uniform distribution of GFP-Arhgap1. Thus, although it is possible that Arhgap1 is transiently reduced or trafficked differently in apical regions of NCCs, localized Rho activation is likely generated through a combination of broad inhibition by Arhgap1 and localized activation in the apical region by as yet unidentified GEFs.

DISCUSSION

Here, we provide the first live imaging of active Rho during EMT in an *in vivo* system. Our experiments have revealed new insight into mechanisms of Rho function in EMT. We find that high Rho levels in a discrete apical region of pre-migratory NCCs generate actomyosin contractile forces to promote apical detachment and drive EMT. Moreover, we have identified Arhgap1 as an essential regulator of Rho activity in NCC EMT.

The mechanisms by which motility is initially generated within an epithelium in the early stages of EMT have been poorly understood. Disruption or modulation of cadherin adhesions is an important step in initiating EMT (Clay and Halloran, 2011; Gumbiner, 2005; Nieto, 2011; Thiery et al., 2009; Wheelock et al., 2008). However, changes in cadherins are not always sufficient to induce EMT, indicating additional signals are required (Derksen et al., 2006; Knudsen et al., 2005; Maeda et al., 2005; Nelson et al., 2008; Park and Gumbiner, 2010). Here, we show that localized apical Rho-ROCK signaling in NCCs drives detachment of cell contacts, initiating motility within the neuroepithelium and EMT. Together with our F-actin localization results, these findings suggest actomyosin contractility acts in concert with disruption of adhesions to drive EMT. This idea is supported by a previous study showing that NCC apical tails can shear during EMT (Ahlstrom and Erickson, 2009), suggesting that active contractile forces are

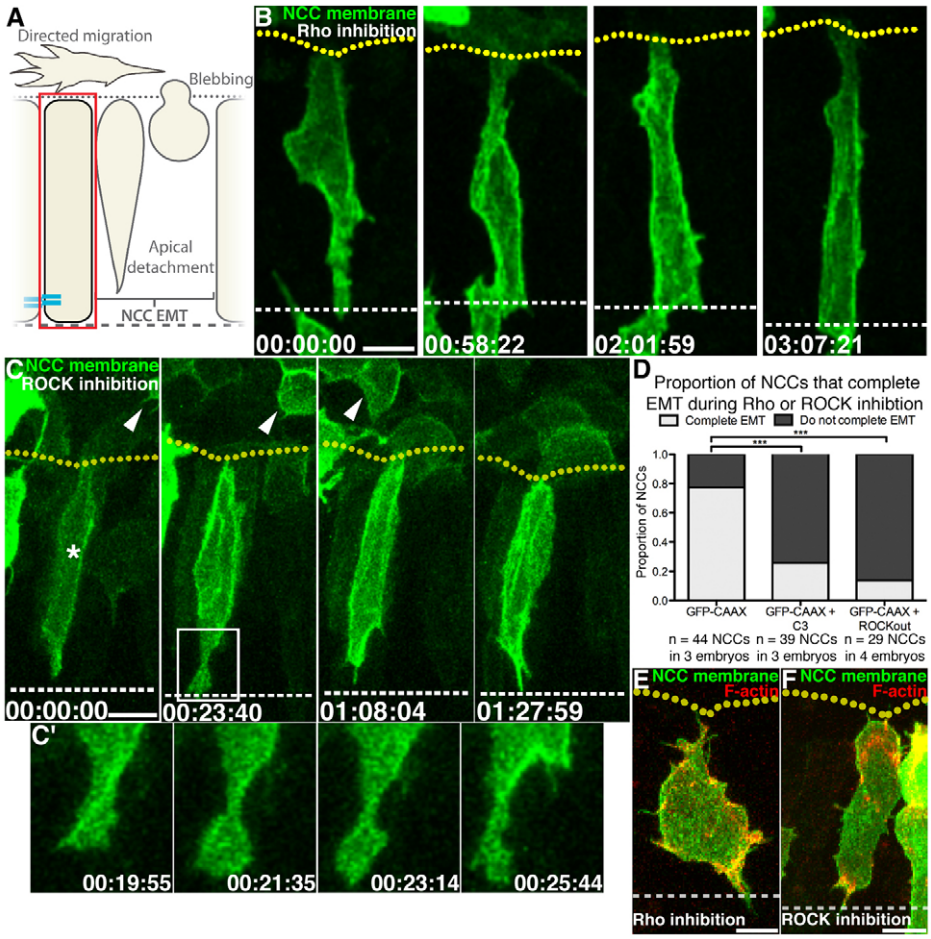

Fig. 5. Rho or ROCK inhibition disrupts apical detachment and NCC EMT. (**A**) Imaging region. (B-C′,E,F) Confocal images (dorsal views, anterior left, *z*-projections). Yellow dotted lines mark basal neuroepithelial surfaces. White dashed lines mark apical midlines. (**B**) Time lapse of a GFP-CAAX-labeled NCC in an embryo treated with C3. NCC does not undergo apical detachment or EMT. (**C**) Time lapse of GFP-CAAX-labeled NCCs in an embryo treated with ROCKout. The NCC in the neuroepithelium (asterisk) does not detach. An NCC that delaminated before imaging migrates anteriorly (arrowheads). Box represents area shown in C′. (**C′**) Protrusive behavior at midline during ROCKout treatment. (**D**) Proportion of labeled NCCs within neuroepithelium completing EMT (***P<0.0001, Fisher's exact test). (**E**,**F**) Single timepoints of premigratory NCCs labeled with GFP-CAAX and mCherry-UtrCH. F-actin accumulates in the apical tail during C3 (E) or ROCKout (F) treatment. Scale bars: 10 μM. Time is given as hours:minutes:seconds.

involved in detachment. Our data reveal a molecular basis for this force, namely Rho-ROCK-dependent contraction. Rho-ROCK forces could act in parallel to cadherin modulation or could directly affect cadherin-based adhesions. Multiple avenues of crosstalk exist between Rho GTPases and cadherins (Braga et al., 1997; Niessen et al., 2011; Samarin and Nusrat, 2009; Yap and Kovacs, 2003), and effects of Rho signaling and contractility on cell junctions can be disparate. Actomyosin forces can be necessary for junctional integrity (le Duc et al., 2010; Nelson and Chen, 2003; Warner and Longmore, 2009a; Warner and Longmore, 2009b; Yonemura et al., 2010), or can disrupt junctions (de Rooij et al., 2005; Samarin et al., 2007; Utech et al., 2005). Complex interactions between Rho, adhesions and tension likely orchestrate EMT, and may create multiple roles for Rho in NCCs and EMT. By showing where and when Rho is active within cells during EMT, and by analyzing how manipulation of Rho signaling affects motile behaviors *in vivo*, we have uncovered a role for Rho in promoting detachment of apical NCC tails.

We also found that Rho is activated in blebs at the basal side of the NCCs during EMT. The pattern of Rho activation is similar to dynamic F-actin in blebs (Berndt et al., 2008), consistent with Rho-generated actomyosin driving NCC bleb retraction. How does actomyosin contractility in different cell locations result in directionality of movement? Contraction at the apical side is coupled with loss of apical adhesions, which results in tail detachment and retraction (Fig. 7). By contrast, blebs contact a very different extracellular environment, including the basal lamina and the ECM of the peripheral mesenchyme, to which cells may adhere and thereby generate traction and forward movement. In primordial germ cells, blebs protrude forward and, as they retract, actomyosin

Table 2. Proportion of cells within the neuroepithelium in contact with the apical and basal surface at 16 hpf

Treatment	Number of embryos	Total number of NCCs in neuroepithelium	Number of apicobasal spanning NCCs	Proportion of apicobasal spanning NCCs	*P*-value (Fisher's exact test; population of comparison noted)
None (wild type)	19	116	35	30.2%	N/A
C3 (2 μg/ml)	15	104	65	62.5%	P<0.0001 (versus wild type)
DMSO (4%)	25	120	30	25.0%	N/A
ROCKout (50 μm)	25	138	90	65.2%	P<0.0001 (versus DMSO)
±Blebbistatin (50 μm)	19	145	89	61.4%	P<0.0001 (versus DMSO)
Control MO (500 μm)	21	199	65	32.4%	N/A
arhGAP1MO1 (750 μm)	21	185	106	57.3%	P<0.0001 (versus control MO)
arhGAP1MO2 (750 μm)	13	136	69	50.7%	P=0.001 (versus control MO)

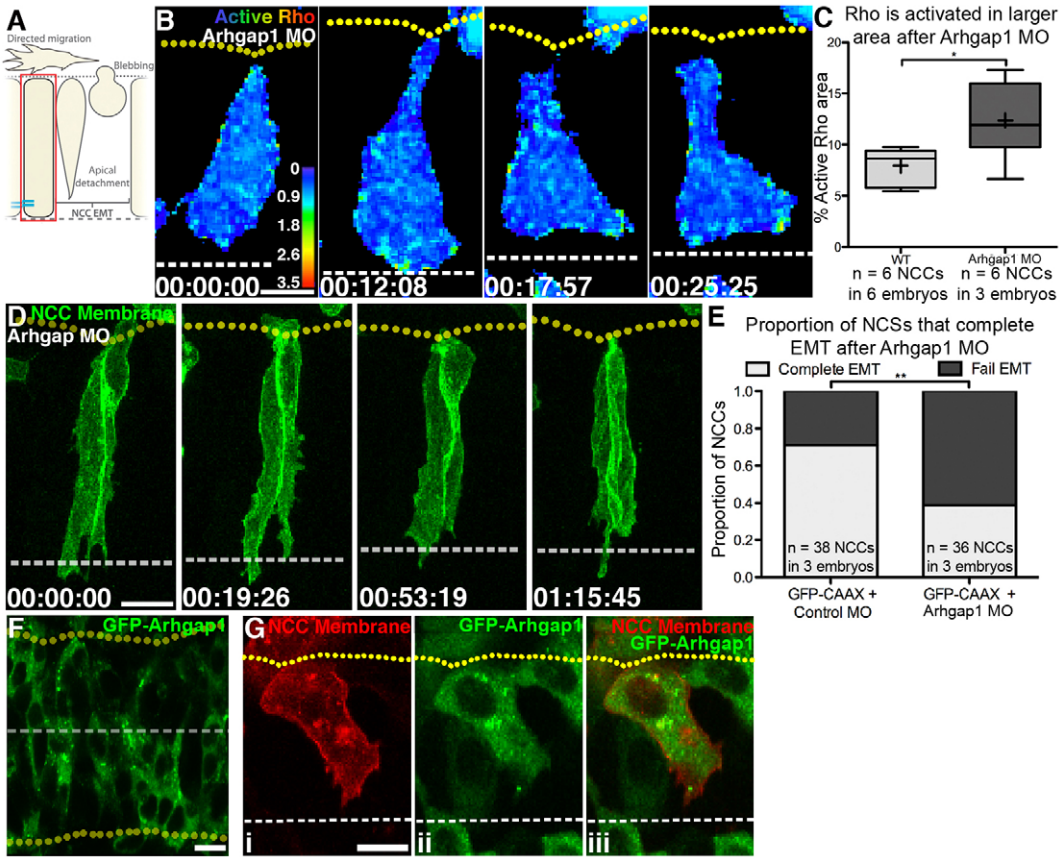

Fig. 6. Arhgap1 knockdown leads to expanded Rho activation and disrupts EMT. (**A**) Imaging region. (B,D,F,G) Confocal images (dorsal views, anterior left, *z*-projections). Yellow dotted lines mark basal neuroepithelial surfaces. White dashed lines mark apical midlines. (**B**) Time lapse of an NCC labeled with GFPrGBD and mCherry in an embryo injected with Arhgap1 morpholino. (**C**) Proportion of total cell area above active Rho threshold (*P<0.05, unpaired two-tailed *t*-test). (**D**) Time lapse of NCCs labeled with GFP-CAAX in an embryo injected with Arhgap1 morpholino. Cells do not undergo detachment or initiate EMT. (**E**) Proportion of labeled NCCs within neuroepithelium completing EMT (**P<0.001 Fisher's exact test). (F,G) Single timepoints of embryos broadly expressing GFP-Arhgap1. (**F**) Neuroepithelial cells show GFP-Arhgap1 throughout cell and in puncta. (**G**) Premigratory NCC labeled with mCherry-CAAX (i, iii) and GFP-Arhgap1 (ii, iii). GFP-Arhgap1 is sometimes decreased in the apical tail. Scale bars: 10 μm. Time is given as hours:minutes:seconds. MO, morpholino.

coupled with adhesion pulls the cell forward (Goudarzi et al., 2012; Kardash et al., 2010). Our data are consistent with NCC blebs driving forward movement in a similar manner. Thus, although the direction of contractile force in NCC apical and basal regions may be opposing, the result is forward motility.

The specific outcome of Rho signaling in NCCs likely depends in part on the level of Rho activation. We show that Rho is activated to the highest levels in the neuroepithelium during EMT and that different levels of activation are associated with different cell behaviors. The lower levels of apical active Rho we see in premigratory NCCs may mediate a function separate from EMT, such as maintenance of epithelial adhesions. Indeed this was suggested as a function for Rho in a previous study that concluded Rho-ROCK signals suppress EMT (Groysman et al., 2008). One potential explanation for the differing findings between that study and ours is that experimental manipulation of Rho does not disrupt all Rho functions equally. Strong inhibition could block all Rho-ROCK functions, including epithelial maintenance, causing epithelial disruption that may resemble EMT. Weaker inhibition may block only the EMT behaviors requiring higher levels of active Rho, mainly affecting EMT. Several differences in experimental conditions between our study and that of Groysman et al. could affect the degree of Rho inhibition and/or experimental outcome, including specific inhibitors used (ROCKout versus Y27632), different time scales of treatments and analyses, different labeling methods (mosaic versus broad), and different experimental preparations. Moreover, distinct populations of NCCs (cranial versus trunk) and NCCs from different species (chick versus zebrafish) can use different mechanisms to complete EMT (Théveneau and Mayor, 2012), and these mechanisms could have different Rho requirements. Thus, although the results of these studies differ, each may describe true biological functions of Rho in NCCs.

The outcome of GTPase signaling in NCCs may be further influenced by the fact that multiple family members are expressed in NCCs at different stages. In chick, RhoB is expressed specifically in NCCs, whereas RhoA is expressed more broadly in the neuroepithelium (Groysman et al., 2008; Liu and Jessell, 1998). In addition, RhoV and RhoU, which do not signal through ROCK, are expressed in *Xenopus* and chick NCCs, and have functions in NCC induction and migration (Fort et al., 2011; Guémar et al., 2007; Notarnicola et al., 2008). In addition, Rac1 promotes chick NCC migration and Rac activation is influenced by Rho (Shoval and Kalcheim, 2012). It will be important to determine how Rho family

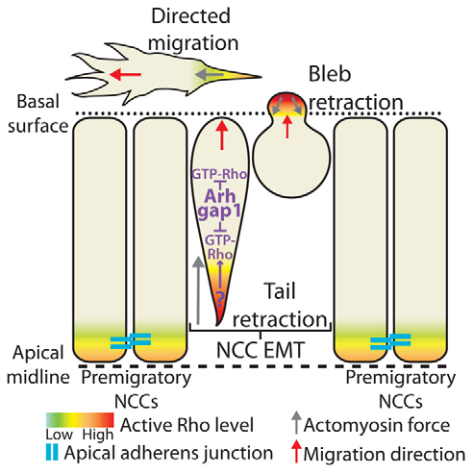

Fig. 7. Rho and Arhgap1 function in hindbrain NCC EMT. Premigratory NCCs have low active Rho in apical tails. Rho is activated to higher levels during EMT, which drives detachment via ROCK and actomyosin. Arhgap1 maintains active Rho distribution by suppressing Rho activation in non-apical regions. During EMT, Rho is also activated in retracting blebs. Once NCCs begin directed migration, active Rho is again decreased in trailing tails.

members function together in NCC EMT and to further uncover the diverse molecular processes that may be used by NCCs in different species and populations to ultimately carry out EMT.

Interestingly, we also found that Rho is activated in trailing edges of migrating NCCs after EMT, but at lower levels than during EMT. This lower Rho activation may reflect previously described functions for Rho in suppressing inappropriate cell protrusions during directed NCC migration after EMT (Carmona-Fontaine et al., 2008; Matthews et al., 2008; Rupp and Kulesa, 2007). The level of active Rho in migrating NCCs is similar to those we observe in apical regions of premigratory NCCs. Thus, even at the same level, Rho activation may regulate multiple cellular functions depending on timing or context.

Not only is the level of active Rho important, but the specific subcellular localization is also a crucial determinant of Rho signaling outcome. In avian gastrulation EMT, Rho is activated in the basal region of epiblast cells prior to EMT by the Rho GEF Net1 (Nakaya et al., 2008). Before EMT, this basally localized Rho maintains the basement membrane, and during EMT it is downregulated, allowing basement membrane degradation. By contrast, we found that, in NCCs, apical localization of Rho activation promotes EMT. Our data fit a model (Fig. 7) in which localized Rho activation focuses the force of actomyosin contraction and drives apical detachment and EMT. We show that Arhgap1 has an essential function in NCC EMT, acting to restrict the localization of Rho activation, presumably by inactivating Rho in non-apical regions. Our finding that Arhgap1 knockdown does not inhibit EMT to the same degree as Rho inhibition suggests that dispersed Rho activation does not have as severe an effect as loss of Rho activity. Indeed, there may be other signals in apical region of NCCs that are unaffected by Arhgap1 knockdown that act to promote detachment. Little is known about how Arhgap1 functions in cell motility processes. In 3D cultures of adenocarcinoma, where Rho GTPase activation is associated with invasion, loss of Arhgap1 decreases invasion (Ahn et al., 2012). This finding was paradoxical because Arhgap1 inactivates RhoGTPases. However, this is consistent with our model of NCC EMT where Arhgap1 does not completely eliminate Rho activation, but rather maintains a balance of Rho activation and focuses signaling to specific subcellular regions. Loss of Arhgap1 also affects migration of mouse embryonic fibroblasts, although this effect is thought to be due to its GAP activity towards Cdc42 because total active Rho levels were unchanged (Yang et al., 2006). However, these studies did not examine whether Rho distribution was altered in Arhgap1 knockout cells. Through live imaging, we have revealed a new function for Arhgap1 in restricting the area of Rho activation within a cell during the crucial process of EMT. Overall, the mechanisms we define here may be used broadly to generate motility in epithelial tissues.

Acknowledgements
We are grateful to Bill Bement for the Rho and F-actin biosensors and for many helpful discussions and comments on the manuscript. We also thank Julie Canman for comments on the manuscript. We thank Hannah Vakilizadeh and Kevin Grunewald for technical assistance, and John Irwin and Kyle Swiggum for fish care.

Funding
This work was supported by National Institutes of Health (NIH) grants [R01NS042228 (M.C.H.), R21NS073114 (M.C.H.) and F31DE022232 (M.R.C.)]. The confocal microscope was acquired with an NIH shared instrumentation grant [S10RR023717]. Deposited in PMC for release after 12 months.

Competing interests statement
The authors declare no competing financial interests.

Author contributions
M.R.C. and M.C.H. designed the experiments. M.R.C. performed the experiments, carried out data analysis and prepared figures. M.R.C. and M.C.H. wrote and edited the manuscript.

Supplementary material
Supplementary material available online at
http://dev.biologists.org/lookup/suppl/doi:10.1242/dev.095448/-/DC1

References

Ahlstrom, J. D. and Erickson, C. A. (2009). The neural crest epithelial-mesenchymal transition in 4D: a 'tail' of multiple non-obligatory cellular mechanisms. *Development* **136**, 1801-1812.
Ahn, Y.-H., Gibbons, D. L., Chakravarti, D., Creighton, C. J., Rizvi, Z. H., Adams, H. P., Pertsemlidis, A., Gregory, P. A., Wright, J. A., Goodall, G. J. et al. (2012). ZEB1 drives prometastatic actin cytoskeletal remodeling by downregulating miR-34a expression. *J. Clin. Invest.* **122**, 3170-3183.
Andersen, E., Asuri, N., Clay, M. and Halloran, M. (2010). Live imaging of cell motility and actin cytoskeleton of individual neurons and neural crest cells in zebrafish embryos. *J. Vis. Exp.* **36**, 1726.
Bakin, A. V., Tomlinson, A. K., Bhowmick, N. A., Moses, H. L. and Arteaga, C. L. (2000). Phosphatidylinositol 3-kinase function is required for transforming growth factor beta-mediated epithelial to mesenchymal transition and cell migration. *J. Biol. Chem.* **275**, 36803-36810.
Barfod, E. T., Zheng, Y., Kuang, W. J., Hart, M. J., Evans, T., Cerione, R. A. and Ashkenazi, A. (1993). Cloning and expression of a human CDC42 GTPase-activating protein reveals a functional SH3-binding domain. *J. Biol. Chem.* **268**, 26059-26062.
Bement, W. M., Benink, H. A. and von Dassow, G. (2005). A microtubule-dependent zone of active RhoA during cleavage plane specification. *J. Cell Biol.* **170**, 91-101.
Benink, H. A. and Bement, W. M. (2005). Concentric zones of active RhoA and Cdc42 around single cell wounds. *J. Cell Biol.* **168**, 429-439.
Berndt, J. D., Clay, M. R., Langenberg, T. and Halloran, M. C. (2008). Rho-kinase and myosin II affect dynamic neural crest cell behaviors during epithelial to mesenchymal transition in vivo. *Dev. Biol.* **324**, 236-244.
Bhowmick, N. A., Ghiassi, M., Bakin, A., Aakre, M., Lundquist, C. A., Engel, M. E., Arteaga, C. L. and Moses, H. L. (2001). Transforming growth factor-beta1 mediates epithelial to mesenchymal transdifferentiation through a RhoA-dependent mechanism. *Mol. Biol. Cell* **12**, 27-36.
Braga, V. M., Machesky, L. M., Hall, A. and Hotchin, N. A. (1997). The small GTPases Rho and Rac are required for the establishment of cadherin-dependent cell-cell contacts. *J. Cell Biol.* **137**, 1421-1431.
Burkel, B. M., von Dassow, G. and Bement, W. M. (2007). Versatile fluorescent probes for actin filaments based on the actin-binding domain of utrophin. *Cell Motil. Cytoskeleton* **64**, 822-832.

Carmona-Fontaine, C., Matthews, H. K., Kuriyama, S., Moreno, M., Dunn, G. A., Parsons, M., Stern, C. D. and Mayor, R. (2008). Contact inhibition of locomotion in vivo controls neural crest directional migration. *Nature* **456**, 957-961.
Cho, H. J. and Yoo, J. Y. (2007). Rho activation is required for transforming growth factor-beta-induced epithelial-mesenchymal transition in lens epithelial cells. *Cell Biol. Int.* **31**, 1225-1230.
Clay, M. R. and Halloran, M. C. (2011). Regulation of cell adhesions and motility during initiation of neural crest migration. *Curr. Opin. Neurobiol.* **21**, 17-22.
Croft, D. R., Sahai, E., Mavria, G., Li, S. X., Tsai, J., Lee, W. M. F., Marshall, C. J. and Olson, M. F. (2004). Conditional ROCK activation in vivo induces tumor cell dissemination and angiogenesis. *Cancer Res.* **64**, 8994-9001.
de Rooij, J., Kerstens, A., Danuser, G., Schwartz, M. A. and Waterman-Storer, C. M. (2005). Integrin-dependent actomyosin contraction regulates epithelial cell scattering. *J. Cell Biol.* **171**, 153-164.
Derksen, P. W. B., Liu, X., Saridin, F., van der Gulden, H., Zevenhoven, J., Evers, B., van Beijnum, J. R., Griffioen, A. W., Vink, J., Krimpenfort, P. et al. (2006). Somatic inactivation of E-cadherin and p53 in mice leads to metastatic lobular mammary carcinoma through induction of anoikis resistance and angiogenesis. *Cancer Cell* **10**, 437-449.
Duband, J. L., Monier, F., Delannet, M. and Newgreen, D. (1995). Epithelium-mesenchyme transition during neural crest development. *Acta Anat. (Basel)* **154**, 63-78.
Fort, P., Guémar, L., Vignal, E., Morin, N., Notarnicola, C., de Santa Barbara, P. and Faure, S. (2011). Activity of the RhoU/Wrch1 GTPase is critical for cranial neural crest cell migration. *Dev. Biol.* **350**, 451-463.
Godsel, L. M., Dubash, A. D., Bass-Zubek, A. E., Amargo, E. V., Klessner, J. L., Hobbs, R. P., Chen, X. Y. and Green, K. J. (2010). Plakophilin 2 couples actomyosin remodeling to desmosomal plaque assembly via RhoA. *Mol. Biol. Cell* **21**, 2844-2859.
Goudarzi, M., Banisch, T. U., Mobin, M. B., Maghelli, N., Tarbashevich, K., Strate, I., van den Berg, J., Blaser, H., Bandemer, S., Paluch, E. et al. (2012). Identification and regulation of a molecular module for bleb-based cell motility. *Dev. Cell* **23**, 210-218.
Groysman, M., Shoval, I. and Kalcheim, C. (2008). A negative modulatory role for rho and rho-associated kinase signaling in delamination of neural crest cells. *Neural Dev.* **3**, 27.
Guémar, L., de Santa Barbara, P., Vignal, E., Maurel, B., Fort, P. and Faure, S. (2007). The small GTPase RhoV is an essential regulator of neural crest induction in Xenopus. *Dev. Biol.* **310**, 113-128.
Guilluy, C., Garcia-Mata, R. and Burridge, K. (2011). Rho protein crosstalk: another social network? *Trends Cell Biol.* **21**, 718-726.
Gumbiner, B. M. (2005). Regulation of cadherin-mediated adhesion in morphogenesis. *Nat. Rev. Mol. Cell Biol.* **6**, 622-634.
Hay, E. D. (1995). An overview of epithelio-mesenchymal transformation. *Acta Anat. (Basel)* **154**, 8-20.
Hong, E. and Brewster, R. (2006). N-cadherin is required for the polarized cell behaviors that drive neurulation in the zebrafish. *Development* **133**, 3895-3905.
Jaffe, A. B. and Hall, A. (2005). Rho GTPases: biochemistry and biology. *Annu. Rev. Cell Dev. Biol.* **21**, 247-269.
Kardash, E., Reichman-Fried, M., Maître, J. L., Boldajipour, B., Papusheva, E., Messerschmidt, E. M., Heisenberg, C. P. and Raz, E. (2010). A role for Rho GTPases and cell-cell adhesion in single-cell motility in vivo. *Nat. Cell Biol.* **12**, 47-53, **Suppl.**, 1-11.
Kimmel, C. B., Ballard, W. W., Kimmel, S. R., Ullmann, B. and Schilling, T. F. (1995). Stages of embryonic development of the zebrafish. *Dev. Dyn.* **203**, 253-310.
Knudsen, K. A., Sauer, C., Johnson, K. R. and Wheelock, M. J. (2005). Effect of N-cadherin misexpression by the mammary epithelium in mice. *J. Cell. Biochem.* **95**, 1093-1107.
Kwan, K. M., Fujimoto, E., Grabher, C., Mangum, B. D., Hardy, M. E., Campbell, D. S., Parant, J. M., Yost, H. J., Kanki, J. P. and Chien, C.-B. (2007). The Tol2kit: a multisite gateway-based construction kit for Tol2 transposon transgenesis constructs. *Dev. Dyn.* **236**, 3088-3099.
Le Douarin, N. M. and Kalcheim, C. (1999). *The Neural Crest*. Cambridge, UK: Cambridge University Press.
le Duc, Q., Shi, Q., Blonk, I., Sonnenberg, A., Wang, N., Leckband, D. and de Rooij, J. (2010). Vinculin potentiates E-cadherin mechanosensing and is recruited to actin-anchored sites within adherens junctions in a myosin II-dependent manner. *J. Cell Biol.* **189**, 1107-1115.
Lessey, E. C., Guilluy, C. and Burridge, K. (2012). From mechanical force to RhoA activation. *Biochemistry* **51**, 7420-7432.
Liu, J. P. and Jessell, T. M. (1998). A role for rhoB in the delamination of neural crest cells from the dorsal neural tube. *Development* **125**, 5055-5067.
López-Novoa, J. M. and Nieto, M. A. (2009). Inflammation and EMT: an alliance towards organ fibrosis and cancer progression. *EMBO Mol. Med.* **1**, 303-314.
Maeda, M., Johnson, K. R. and Wheelock, M. J. (2005). Cadherin switching: essential for behavioral but not morphological changes during an epithelium-to-mesenchyme transition. *J. Cell Sci.* **118**, 873-887.
Martin, A. C. (2010). Pulsation and stabilization: contractile forces that underlie morphogenesis. *Dev. Biol.* **341**, 114-125.
Masszi, A., Di Ciano, C., Sirokmany, G., Arthur, W. T., Rotstein, O. D., Wang, J. X., McCulloch, C. A. G., Rosivall, L., Mucsi, I. and Kapus, A. (2003). Central role for Rho in TGF-beta(1)-induced alpha-smooth muscle actin expression during epithelial-mesenchymal transition. *Am. J. Physiol.* **284**, F911-F924.
Matthews, H. K., Marchant, L., Carmona-Fontaine, C., Kuriyama, S., Larraín, J., Holt, M. R., Parsons, M. and Mayor, R. (2008). Directional migration of neural crest cells in vivo is regulated by Syndecan-4/Rac1 and non-canonical Wnt signaling/RhoA. *Development* **135**, 1771-1780.
Miller, A. L. and Bement, W. M. (2009). Regulation of cytokinesis by Rho GTPase flux. *Nat. Cell Biol.* **11**, 71-77.
Nakaya, Y., Sukowati, E. W., Wu, Y. and Sheng, G. (2008). RhoA and microtubule dynamics control cell-basement membrane interaction in EMT during gastrulation. *Nat. Cell Biol.* **10**, 765-775.
Nelson, C. M. and Chen, C. S. (2003). VE-cadherin simultaneously stimulates and inhibits cell proliferation by altering cytoskeletal structure and tension. *J. Cell Sci.* **116**, 3571-3581.
Nelson, C. M., Khauv, D., Bissell, M. J. and Radisky, D. C. (2008). Change in cell shape is required for matrix metalloproteinase-induced epithelial-mesenchymal transition of mammary epithelial cells. *J. Cell. Biochem.* **105**, 25-33.
Niessen, C. M., Leckband, D. and Yap, A. S. (2011). Tissue organization by cadherin adhesion molecules: dynamic molecular and cellular mechanisms of morphogenetic regulation. *Physiol. Rev.* **91**, 691-731.
Nieto, M. A. (2002). The snail superfamily of zinc-finger transcription factors. *Nat. Rev. Mol. Cell Biol.* **3**, 155-166.
Nieto, A. (2011). The ins and outs of the epithelial to mesenchymal transition in health and disease. In *Annual Review of Cell and Developmental Biology* (ed. R. G. L. L. R. Schekman), pp. 347-376.
Notarnicola, C., Le Guen, L., Fort, P., Faure, S. and de Santa Barbara, P. (2008). Dynamic expression patterns of RhoV/Chp and RhoU/Wrch during chicken embryonic development. *Dev. Dyn.* **237**, 1165-1171.
Ouchida, M., Kanzaki, H., Ito, S., Hanafusa, H., Jitsumori, Y., Tamaru, S. and Shimizu, K. (2012). Novel direct targets of miR-19a identified in breast cancer cells by a quantitative proteomic approach. *PLoS ONE* **7**, e44095.
Ozdamar, B., Bose, R., Barrios-Rodiles, M., Wang, H. R., Zhang, Y. and Wrana, J. L. (2005). Regulation of the polarity protein Par6 by TGFbeta receptors controls epithelial cell plasticity. *Science* **307**, 1603-1609.
Park, K. S. and Gumbiner, B. M. (2010). Cadherin 6B induces BMP signaling and de-epithelialization during the epithelial mesenchymal transition of the neural crest. *Development* **137**, 2691-2701.
Peng, J., Zhang, G., Wang, Q. S., Huang, J. G., Ma, H., Zhong, Y. H., Zhou, F. X., Xie, C. H. and Zhang, A. (2012). ROCK cooperated with ET-1 to induce epithelial to mesenchymal transition through SLUG in human ovarian cancer cells. *Biosci. Biotechnol. Biochem.* **76**, 42-47.
Provenzano, P. P. and Keely, P. J. (2011). Mechanical signaling through the cytoskeleton regulates cell proliferation by coordinated focal adhesion and Rho GTPase signaling. *J. Cell Sci.* **124**, 1195-1205.
Ridley, A. J., Self, A. J., Kasmi, F., Paterson, H. F., Hall, A., Marshall, C. J. and Ellis, C. (1993). rho family GTPase activating proteins p190, bcr and rhoGAP show distinct specificities in vitro and in vivo. *EMBO J.* **12**, 5151-5160.
Rohani, N., Canty, L., Luu, O., Fagotto, F. and Winklbauer, R. (2011). EphrinB/EphB signaling controls embryonic germ layer separation by contact-induced cell detachment. *PLoS Biol.* **9**, e1000597.
Rupp, P. A. and Kulesa, P. M. (2007). A role for RhoA in the two-phase migratory pattern of post-otic neural crest cells. *Dev. Biol.* **311**, 159-171.
Sahai, E. and Marshall, C. J. (2003). Differing modes of tumour cell invasion have distinct requirements for Rho/ROCK signalling and extracellular proteolysis. *Nat. Cell Biol.* **5**, 711-719.
Samarin, S. and Nusrat, A. (2009). Regulation of epithelial apical junctional complex by Rho family GTPases. *Front. Biosci.* **14**, 1129-1142.
Samarin, S. N., Ivanov, A. I., Flatau, G., Parkos, C. A. and Nusrat, A. (2007). Rho/Rho-associated kinase-II signaling mediates disassembly of epithelial apical junctions. *Mol. Biol. Cell* **18**, 3429-3439.
Shook, D. and Keller, R. (2003). Mechanisms, mechanics and function of epithelial-mesenchymal transitions in early development. *Mech. Dev.* **120**, 1351-1383.
Shoval, I. and Kalcheim, C. (2012). Antagonistic activities of Rho and Rac GTPases underlie the transition from neural crest delamination to migration. *Dev. Dyn.* **241**, 1155-1168.
Sirokmány, G., Szidonya, L., Káldi, K., Gáborik, Z., Ligeti, E. and Geiszt, M. (2006). Sec14 homology domain targets p50RhoGAP to endosomes and provides a link between Rab and Rho GTPases. *J. Biol. Chem.* **281**, 6096-6105.
Tcherkezian, J. and Lamarche-Vane, N. (2007). Current knowledge of the large RhoGAP family of proteins. *Biol. Cell* **99**, 67-86.
Théveneau, E. and Mayor, R. (2012). Neural crest delamination and migration: from epithelium-to-mesenchyme transition to collective cell migration. *Dev. Biol.* **366**, 34-54.

Thiery, J. P., Acloque, H., Huang, R. Y. and Nieto, M. A. (2009). Epithelial-mesenchymal transitions in development and disease. *Cell* **139**, 871-890.
Thisse, B. and Thisse, C. (2004). Fast release clones: a high throughput expression analysis. zfin direct data submission. http://zfin.org.
Utech, M., Ivanov, A. I., Samarin, S. N., Bruewer, M., Turner, J. R., Mrsny, R. J., Parkos, C. A. and Nusrat, A. (2005). Mechanism of IFN-gamma-induced endocytosis of tight junction proteins: myosin II-dependent vacuolarization of the apical plasma membrane. *Mol. Biol. Cell* **16**, 5040-5052.
Vaughan, E. M., Miller, A. L., Yu, H. Y. E. and Bement, W. M. (2011). Control of local Rho GTPase crosstalk by Abr. *Curr. Biol.* **21**, 270-277.
von Dassow, G., Verbrugghe, K. J. C., Miller, A. L., Sider, J. R. and Bement, W. M. (2009). Action at a distance during cytokinesis. *J. Cell Biol.* **187**, 831-845.
Wada, N., Javidan, Y., Nelson, S., Carney, T. J., Kelsh, R. N. and Schilling, T. F. (2005). Hedgehog signaling is required for cranial neural crest morphogenesis and chondrogenesis at the midline in the zebrafish skull. *Development* **132**, 3977-3988.
Wang, L., Yang, L., Burns, K., Kuan, C.-Y. and Zheng, Y. (2005). Cdc42GAP regulates c-Jun N-terminal kinase (JNK)-mediated apoptosis and cell number during mammalian perinatal growth. *Proc. Natl. Acad. Sci. USA* **102**, 13484-13489.
Wang, L., Yang, L., Filippi, M. D., Williams, D. A. and Zheng, Y. (2006). Genetic deletion of Cdc42GAP reveals a role of Cdc42 in erythropoiesis and hematopoietic stem/progenitor cell survival, adhesion, and engraftment. *Blood* **107**, 98-105.
Warner, S. J. and Longmore, G. D. (2009a). Cdc42 antagonizes Rho1 activity at adherens junctions to limit epithelial cell apical tension. *J. Cell Biol.* **187**, 119-133.
Warner, S. J. and Longmore, G. D. (2009b). Distinct functions for Rho1 in maintaining adherens junctions and apical tension in remodeling epithelia. *J. Cell Biol.* **185**, 1111-1125.
Wheelock, M. J., Shintani, Y., Maeda, M., Fukumoto, Y. and Johnson, K. R. (2008). Cadherin switching. *J. Cell Sci.* **121**, 727-735.
Wilkinson, S., Paterson, H. F. and Marshall, C. J. (2005). Cdc42-MRCK and Rho-ROCK signalling cooperate in myosin phosphorylation and cell invasion. *Nat. Cell Biol.* **7**, 255-261.
Yang, L., Wang, L. and Zheng, Y. (2006). Gene targeting of Cdc42 and Cdc42GAP affirms the critical involvement of Cdc42 in filopodia induction, directed migration, and proliferation in primary mouse embryonic fibroblasts. *Mol. Biol. Cell* **17**, 4675-4685.
Yap, A. S. and Kovacs, E. M. (2003). Direct cadherin-activated cell signaling: a view from the plasma membrane. *J. Cell Biol.* **160**, 11-16.
Yonemura, S., Wada, Y., Watanabe, T., Nagafuchi, A. and Shibata, M. (2010). alpha-Catenin as a tension transducer that induces adherens junction development. *Nat. Cell Biol.* **12**, 533-542.
Zhang, B. and Zheng, Y. (1998). Regulation of RhoA GTP hydrolysis by the GTPase-activating proteins p190, p50RhoGAP, Bcr, and 3BP-1. *Biochemistry* **37**, 5249-5257.

Fig. S1

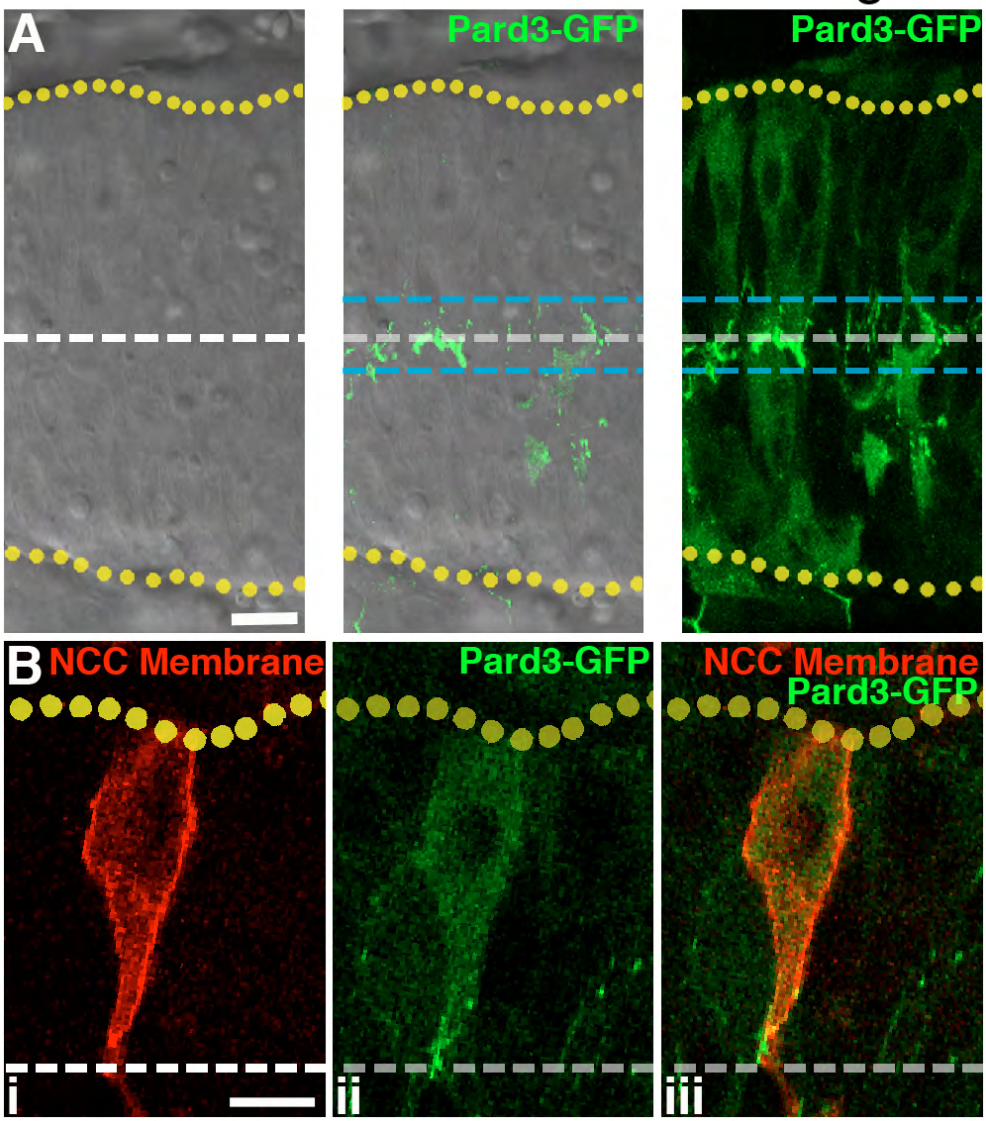

Fig. S1. Premigratory NCC tails, identified by the embryonic midline, express the apical marker Pard3-GFP. (**A**,**B**) Confocal images of single timepoints in live embryos (dorsal views, anterior left). Yellow dotted lines mark basal surfaces of the neuroepithelium and white dashed lines mark apical midlines, identified by DIC. (A) Single plane of DIC (i, ii) in an embryo broadly expressing Pard3-GFP (*z*-projection, ii, iii). The blue dashed lines (ii, iii) are 5 μm from the midline and the majority of Pard3-GFP is observed in this area. (B) Single plane of NCCs expressing mCherry-CAAX (i, iii) and Pard3-GFP (ii, iii). The NCC was identified as premigratory (tail at the midline) and the tail showed the apical marker Pard3-GFP. Scale bars: 10 μm.

Fig. S2

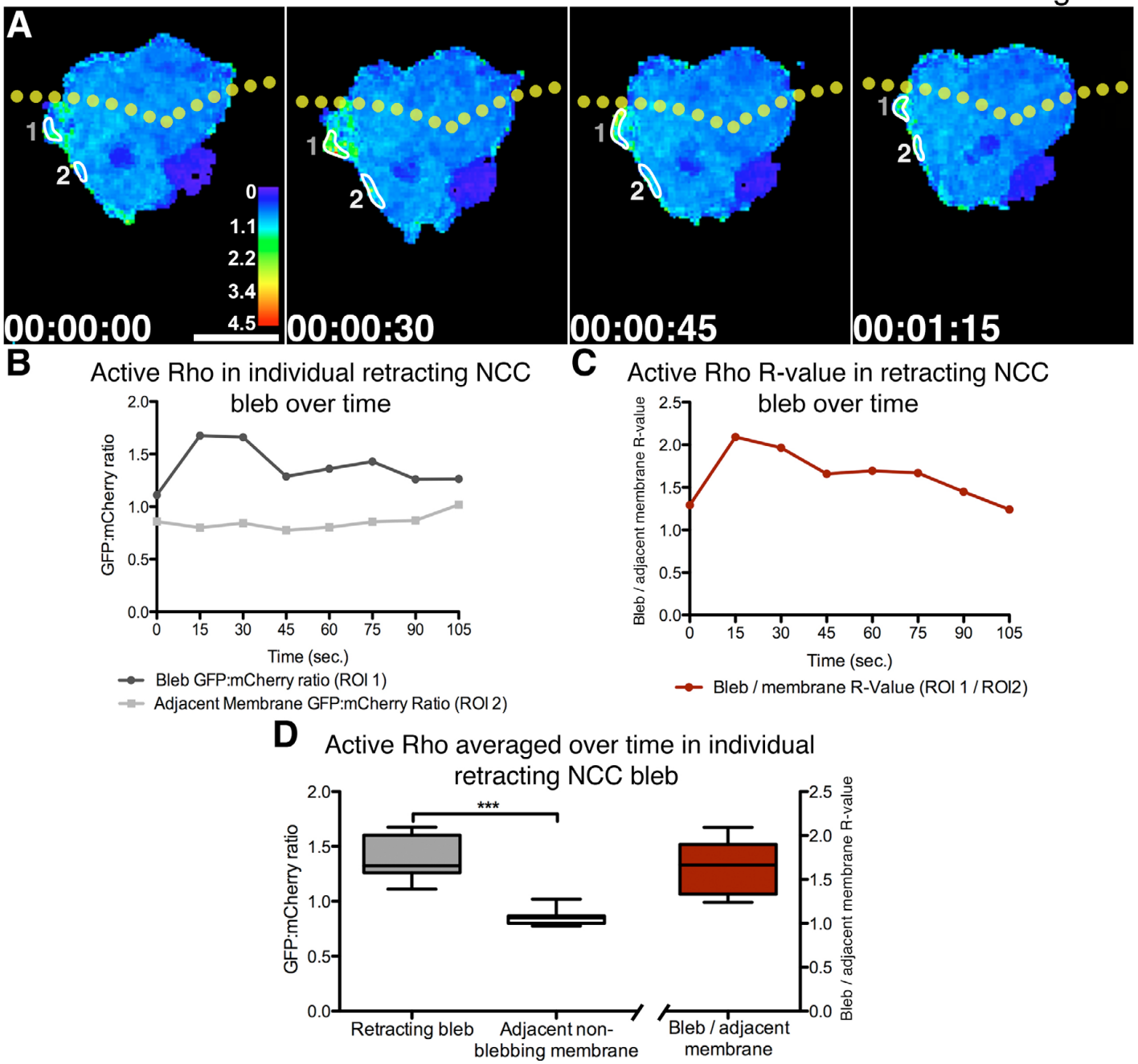

Fig. S2. Calculation of R-values in NCC bleb. (**A**) Time-lapse images (dorsal views, anterior left, confocal z-projections) of NCC labeled with GFPrGBD and mCherry. ROIs were used to calculate GFP/mCherry intensity in blebbing (1) and non-blebbing (2) membrane. Look-up table shows GFP/mCherry intensity. Yellow dotted lines mark the basal neuroepithelium. (**B**) GFP/mCherry intensity in bleb (dark line) and non-blebbing membrane (light line) over time beginning at time of maximum bleb extension for cell shown in A. (**C**) Active Rho R-values (ROI1/ROI2) plotted over time. (**D**) Average GFP/mCherry intensity over time is significantly higher in blebbing than non-blebbing membrane (left axis, ***P<0.001, paired one-tailed, t-test, see Table S1 for all blebs). Average of active Rho R-values (right axis) is 1.62 (62% higher active Rho in bleb). Scale bar: 10 μm.

Fig. S3

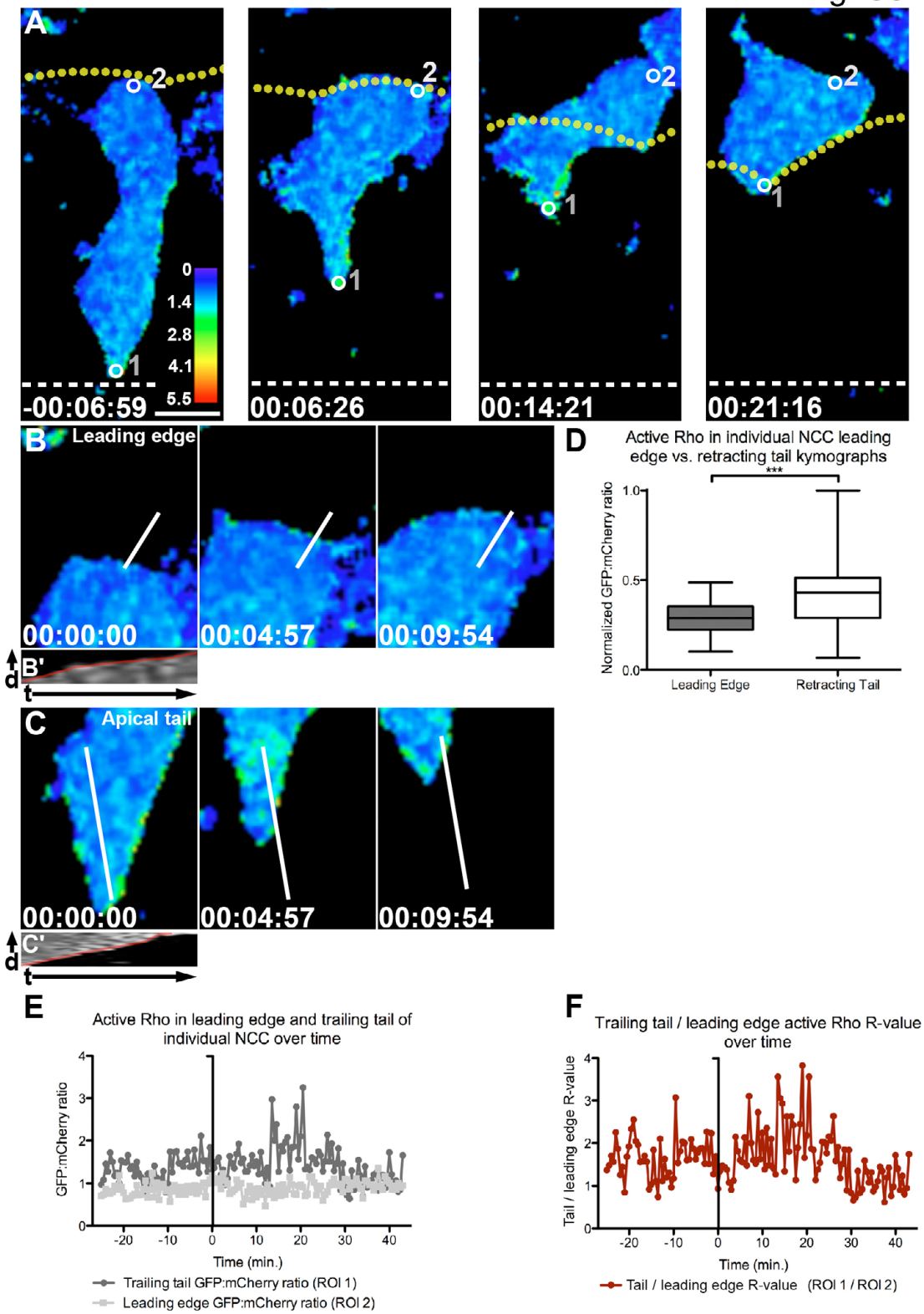

Fig. S3. Calculation of R-values in NCC tail. (**A**) Time-lapse images (dorsal views, anterior left, confocal z-projections) of NCCs labeled with GFPrGBD and mCherry. Circles show ROIs used to calculate GFP/mCherry intensity in NCC tail (1) and leading edge (2). Look-up table shows GFP:mCherry ratio intensity. Yellow dotted lines mark the basal surface of the neuroepithelium and white dashed lines mark the apical midline. In A,B,C,E,F, apical detachment is 0 minutes. (**B**,**C**) Higher magnification views of leading edge and tail, showing lines used for kymographs. (**B′**,**C′**) Kymographs of normalized GFP/mCherry intensity over time. The red line represents the border of the cell on the kymograph. GFP/mCherry intensity was measured along this line and averaged to determine the active Rho level. (**D**) Average normalized GFP/mCherry intensity in tail (from C′) was significantly higher than the leading edge (from B′; ***P<0.001, paired one-tailed, t-test, see Table S2 for all tail retraction events). (**E**) GFP/mCherry intensity for the tail (dark line) and leading edge (light line) over time for individual NCCs. (**F**) Active Rho R-value (ROI1/ROI2) plotted over time. Scale bar: 10 μm.

Fig. S4

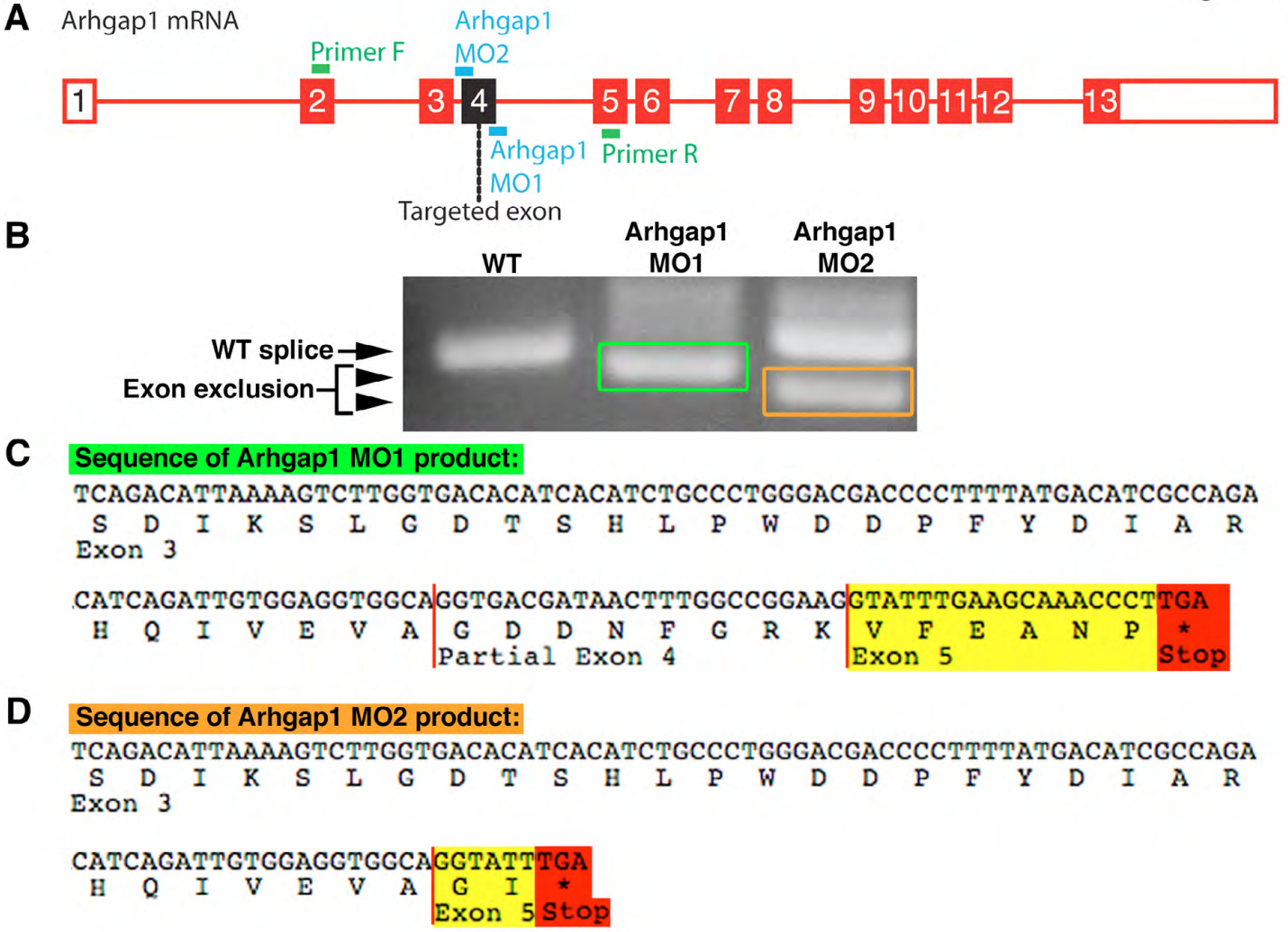

Fig. S4. Morpholinos against Arhgap1 disrupt normal splicing. (**A**) Schematic of zebrafish Arhgap1. Exons are numbered and open boxes represent untranslated regions. Morpholino target sites and primers for PCR from cDNA are shown. (**B**) Arhgap1 PCR products using cDNA from uninjected (wild type), Arhgap1 MO-1- and Arhgap1 MO-2-injected embryos. Both morpholinos result in smaller bands, which correspond to exon exclusion. MO-2 also showed a band corresponding to wild-type Arhgap1 splicing. (C,D) Sequence of PCR products resulting from morpholino injections. (**C**) Arhgap1 MO-1 injection resulted in exclusion of most of exon 4; however, it appears a cryptic splice site was found. The missplicing resulted in a frame shift (highlighted in yellow) and a premature stop (red). (**D**) Arhgap1 MO-2 injection resulted in complete exclusion of exon 4 and introduced a frame shift (yellow) and premature stop (red).

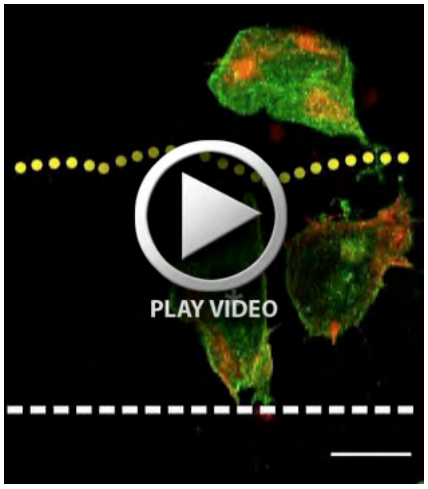

Movie 1. F-Actin transiently accumulates in NCC tails prior to detachment. Movie of NCCs labeled with GFP-CAAX and mCherry-UtrCH. Images were acquired every 30 seconds; movie shows 63 minutes. In the first frame, the cell marked with the asterisk is in a premigratory morphology; the yellow dotted line marks the basal surface of the neuroepithelium; the white dashed line marks the midline. Scale bar: 10 μm.

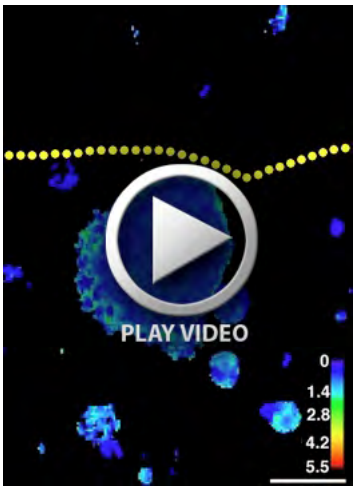

Movie 2. Rho is activated in retracting NCC blebs. Movie of NCCs labeled with GFPrGBD and mCherry. The ratio channel of GFP:mCherry is shown. Images were captured every 10 seconds; movie shows 4 minutes. In the first frame, the yellow dotted line marks the basal surface of the neuroepithelium; the look-up table shows the GFP:mCherry ratio. Scale bar: 10 μm.

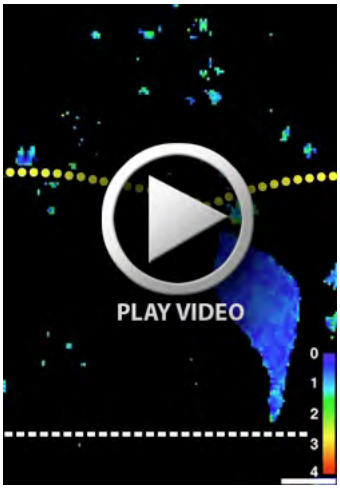

Movie 3. Rho is activated in apical tails prior to detachment and during tail retraction. Movie of NCCs labeled with GFPrGBD and mCherry. The ratio channel of GFP:mCherry is shown. Images were acquired every 30 seconds; movie shows 75 minutes. In the first frame, the yellow dotted line marks the basal surface of the neuroepithelium; the white dashed line marks the midline; the look-up table shows the GFP:mCherry ratio. Scale bar: 10 μm.

Movie 4. Apical NCC tail detachment is disrupted during C3 treatment. Movie of NCC labeled with GFP-CAAX treated with C3. Images were acquired every 30 seconds; movie shows 123 minutes. In the first frame, the yellow dotted line marks the basal surface of the neuroepithelium; the white dashed line marks the midline. Scale bar: 10 μm.

Movie 5. Apical tail detachment is disrupted during ROCKout treatment. Movie of NCCs labeled with GFP-CAAX treated with ROCKout. Images were acquired every 30 seconds; movie shows 171 minutes. In the first frame, the yellow dotted lines mark the basal surface of the neuroepithelium; the white dashed line marks the midline. Scale bar: 10 μm.

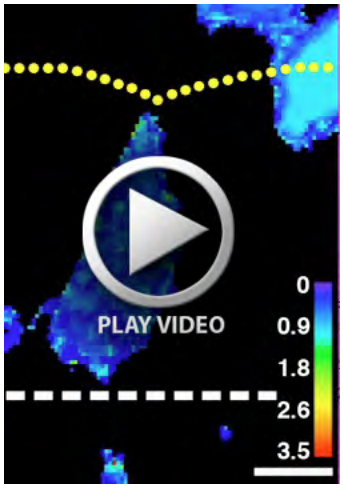

Movie 6. Arhgap1 knockdown leads to expanded Rho activation. Movie of NCCs expressing GFPrGBD and mCherry in embryos injected with Arhgap1 morpholino. Images were acquired every 30 seconds; movie shows 26 minutes. In the first frame, the yellow dotted lines mark the basal surface of the neuroepithelium; the white dashed line marks the midline; the look-up table shows the GFP:mCherry ratio. Scale bar: 10 μm.

Table S1. Comparison of active Rho GFP/mCherry intensity averaged over time in retracting blebs versus adjacent non-blebbing membrane

	GFP/mCherry intensity averaged over time				
Bleb number	Bleb ratio (mean)	s.d.	Adjacent membrane ratio (mean)	s.d.	*P* value (paired *t*-test, bleb versus membrane)
1	0.99	0.17	0.54	0.18	0.0387
2	1.04	0.10	0.83	0.03	0.0044
3	1.21	0.12	0.68	0.09	0.0006
4	0.79	0.12	0.66	0.04	0.1413
5	0.96	0.08	0.80	0.05	0.014
6	0.92	0.06	0.71	0.05	0.0122
7	1.09	0.22	0.87	0.04	0.087
8	1.53	0.13	0.96	0.09	<0.0001
9	1.66	0.19	0.82	0.04	0.0004
10	1.56	0.18	0.96	0.07	0.0025
11	1.82	0.49	1.05	0.13	0.006
12	0.97	0.07	0.74	0.06	0.0061
13	1.01	0.11	0.84	0.03	0.0493
14	1.38	0.20	0.87	0.11	0.0002
15	1.31	0.25	0.85	0.06	0.0304

Table S2. Comparison of active Rho over time averaged in leading edge versus trailing tail as measured from kymographs

Retraction event	Normalized GFP/mCherry intensity over time				
	Leading edge	s.d.	Trailing tail	s.d.	*P* value (paired *t*-test, leading versus trailing edge)
1	0.30	0.17	0.52	0.13	<0.0001
2*	0.29	0.08	0.41	0.16	<0.0001
3*	0.43	0.11	0.61	0.14	<0.0001
4*	0.41	0.08	0.52	0.27	<0.0001
5	0.60	0.12	0.66	0.20	<0.0001
6	0.24	0.06	0.32	0.19	<0.0001
7	0.40	0.04	0.50	0.17	<0.0001
8*	0.26	0.08	0.58	0.13	< 0.0001
9	0.37	0.05	0.47	0.17	<0.0001
10	0.37	0.09	0.70	0.14	<0.0001

*Indicates apical detachment